OAK RIDGE NATIONAL LABORATORY
operated by
UNION CARBIDE CORPORATION
NUCLEAR DIVISION
for the
U.S. ATOMIC ENERGY COMMISSION

ORNL - TM - 1896

HYDROMAGNETIC STABILIZATION OF JET-DRIVEN VORTEX FLOW

J. J. Keyes, Jr.
T. S. Chang
W. K. Sartory

DISCLAIMER

ORNL-TM-1896

Contract No. W-7405-eng-26

Reactor Division

HYDROMAGNETIC STABILIZATION OF JET-DRIVEN VORTEX FLOW

J. J. Keyes, Jr., T. S. Chang, and W. K. Sartory

OCTOBER 1967

OAK RIDGE NATIONAL LABORATORY
Oak Ridge, Tennessee
operated by
UNION CARBIDE CORPORATION
for the
U. S. ATOMIC ENERGY COMMISSION

THIS PAGE

WAS INTENTIONALLY

LEFT BLANK

CONTENTS

HYDROMAGNETIC STABILIZATION OF JET-DRIVEN VORTEX FLOW

J. J. Keyes, Jr., T. S. Chang,† and W. K. Sartory

ABSTRACT

Confined, vortex-type flows generated by tangential impingement of fluid on the interior surface of a tube are observed to be unstable at values of tangential Reynolds modulus much below the range of interest for such advanced energy conversion applications as the gaseous-fueled nuclear reactor and the vortex magnetohydrodynamic power generator. At the operating temperature level envisioned for these devices, however, the electrical conductivity may be sufficiently high that magnetohydrodynamic stabilization can be considered. Experiments are described which demonstrate the stabilizing influence of an axial magnetic field (up to 75 kilogauss) on vortex flow of an aqueous electrolytic conductor generated by two-dimensional, tangential wall jets. For example, using a 10-cm-diam vortex tube having two feed jets and a single exit orifice at the center of one end, the tangential Reynolds modulus at transition to instability was increased from 500 with no magnetic field to 7600 with the 75 kilogauss field (corresponding to a Hartmann modulus based on the tube radius of 172). The experimental magnetic stabilization results for 1-, 2-, and 4-slit injection are correlated in terms of a modified "Görtler modulus" [tangential Reynolds modulus based on momentum boundary-layer thickness times (momentum thickness/radius)$^{0.43}$] and the Hartmann modulus based on momentum thickness.

An MHD Görtler-type stability analysis based on a tangential jet-injection velocity profile over a concave wall is considered. The fluid medium is assumed to be incompressible, viscous, and electrically conducting. The stationary jet-injection velocity profile is calculated according to the classical theory of laminar boundary-layer flow, neglecting effects of curvature. The stability analysis is carried out numerically based on the linear perturbation theory for the calculated stationary profile subjected to an external magnetic field. Whereas the jet-velocity recovery ratios (tangential velocity extrapolated to wall/mean injection velocity) derived from the theoretical stationary velocity profiles agree well with the measurements for magnetically stabilized vortex flow, the agreement between results of the stability analysis and the measurements is poor. Possible reasons for the disagreement are discussed.

---

†Consultant, Heat Transfer—Fluid Mechanics Section, Engineering Science Department, Reactor Division; NSF Professor of Continuum Mechanics, Department of Engineering Mechanics, North Carolina State University, Raleigh, North Carolina.

1. INTRODUCTION

Confined, vortex-like flows generated by tangential impingement of fluid on the interior surface of a tube are of current interest for application to such advanced energy conversion devices as the vortex magnetohydrodynamic (MHD) generator and the gaseous fuel (or gas-core) nuclear reactor utilizing vortex containment of the fissionable material. The vortex MHD generator, for example, utilizes the interaction between a rotating plasma and an axial (or radial) magnetic field to induce a radial (or axial) electric field.[1] The vortex gaseous-fuel reactor, as originally proposed, depends on a balance between the outward centrifugal force on the heavy fuel molecules and the inward force due to convection of a light gas which is used to generate the vortex and which spirals radially inward. This balance of forces can, in principle for laminar flow, effect containment of the fuel in an annular region away from the cylindrical wall within which the gas is constrained to rotate, thereby enabling gas temperatures to be attained which may be well in excess of that for solid-fuel reactors.[2]

It may be possible to combine the vortex reactor and the vortex MHD generator in the same tubular unit, as illustrated schematically in Fig. 1. Here the vortex flow field is generated by jets of light gas impinging tangentially on the concave interior surface of a straight channel, in this case a unit cell of the reactor core matrix. The gas spirals radially inward through the annular fuel zone and, in the process, is heated by direct molecular interchange and/or radiation. The hot, rotating gas which may be strongly ionized and hence electrically conducting (i.e., a plasma) will interact with an axial magnetic field

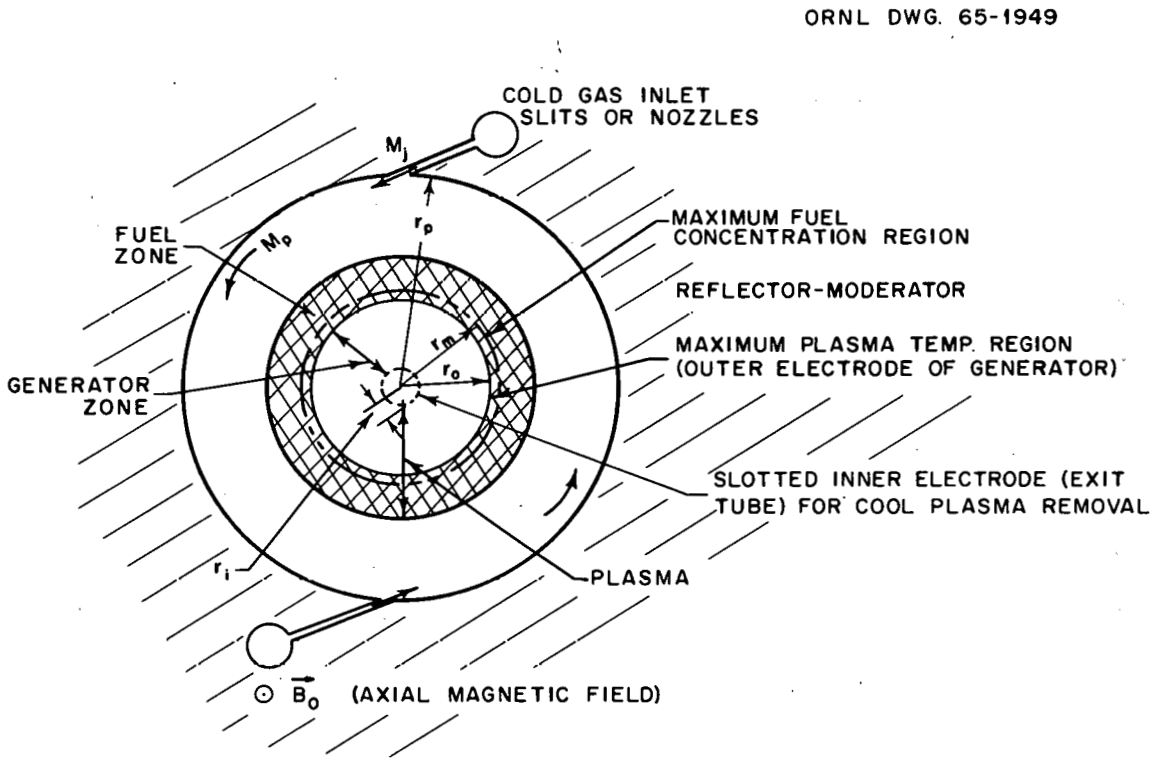

Fig. 1. Integral Vortex Reactor–MHD Generator Concept.

to produce a radial electric field between the inner electrode (which also serves for removal of the gas) and the fuel zone which would serve as an outer plasma electrode for the vortex generator.

Experimental studies of jet-driven vortex-type flows have revealed that such flows are turbulent at values of tangential velocity (and corresponding tangential Reynolds modulus) much below the range of interest for the applications.[3] Turbulence results in excessive frictional losses, and, in the case of the reactor application, limits separation and hence fuel containment by the process of eddy mixing. Suppression of or, hopefully, complete elimination of turbulence would certainly increase the feasibility of these energy conversion concepts. Another problem of hydrodynamic origin results from the interaction of the primary tangential flow with the end walls of the vortex chamber causing some of the fuel mixture to bypass the interior of the chamber by radial flow in the boundary layers which develop on the end walls. This problem was considered analytically and experimentally by Kidd.[4]

Attempts to minimize turbulence by purely fluid-mechanical techniques, such as wall suction employing porous and slotted walls, and wall cooling, have met with only limited success.[3-5] Most recently, however, attention has been focused on the stabilizing influence of an axial magnetic field on the vortex flow of an electrically conducting fluid since, in the applications of interest, operation will be at sufficiently high temperature to sustain a relatively high level of ionization in an inert gas (for example, helium seeded with cesium). This paper summarizes results of an exploratory analytical and experimental investigation into confined, vortex-like flow of an electrically

conducting fluid for the ultimate purpose of determinging the feasibility of applying magnetic stabilization to the vortex reactor concept and extending significantly the initial results reported by Keyes.[6-7] The term vortex-like flow is used here to describe a flow which is predominantly two dimensional over most of the chamber volume and which is characterized by a tangential velocity which varies approximately inversely with radius (free vortex) away from solid boundaries. As a consequence of the reduction in wall shear effected by stabilization of the flow, increase in recovery of injection velocity as tangential velocity would be expected; and this paper also presents experimental and analytical results substantiating this expectation.

2. LITERATURE REVIEW

To the authors' knowledge, no experimental hydromagnetic investigation into jet-driven vortex flows other than that described by Keyes has been reported. Some work has been described, however, in which the stabilizing effect of an axial magnetic field on axisymmetric Couette flow was experimentally determined. The most significant results appear to be those of Donnelly and Ozima[8] and of Donnelly and Caldwell[9] who employed a rotating cylinder viscometer (relatively small gap) in which the inner cylinder was rotated at constant speed and the torque transmitted to the stationary outer cylinder was measured; mercury was used as the electrically conducting fluid. The observed dependence of the critical Taylor modulus on Hartmann modulus for the case of plastic, insulated cylinders, agreed very closely

with the theory of Chandrasekhar[10] for insulating walls (Taylor modulus proportional to the square of the Hartmann modulus).

Recently Chang and Sartory[11] have developed criteria for hydromagnetic stability of non-dissipative and dissipative incompressible vortex-like flows including effects of inward and outward radial flow, under the assumption that transition occurs from a stationary two-dimensional flow to a stationary, three-dimensional flow of cellular nature as described originally by G. I. Taylor. For the case of perfectly conducting nonpermeable walls, it can be deduced that the critical tangential Reynolds modulus for transition to instability increases as the square of the Hartmann modulus (dimensionless magnetic field strength defined in Section 4) for sufficiently large values of the Hartmann modulus. It is now known, however, that under certain conditions transition to oscillatory modes of instability can occur which lead to lower critical Reynolds moduli than those based on stationary modes. The analysis of oscillatory modes is summarized by Chang and Sartory in Ref. 12, from which it can be deduced that, for the case just considered, the oscillatory modes are more critical and lead to an asymptotic relationship between tangential Reynolds modulus and Hartmann modulus which is linear. The main implication of these hydromagnetic Couette flow results as far as the present problem is concerned is that, if the instability in the jet-driven case is derived from the same mechanism as the Taylor instability (or more appropriately the Taylor-Görtler instability), it would be reasonable to expect a similar stabilizing influence of the magnetic field.

The assumption of axisymmetric Couette flow between rotating cylinders is not a particularly good approximation to the actual jet-driven flow of interest for the applications. Rather, the actual flow is dominated by a boundary layer which forms downstream from a tangential wall jet impinging on a curved surface. This flow is certainly not axisymmetric, although there is circumferential periodicity associated with the uniformly spaced jets. Initial results are presented in Section 5 of an analysis which considers the jet-boundary layer with respect to both stationary velocity distribution and hydromagnetic stability; these analytical results are compared with the experimental data in Sections 4 and 5.

In connection with the use of an aqueous electrolytic conductor as the working fluid, the investigation of Boedeker and Covert[13] is of significance. They measured the effect of a transverse magnetic field on the helical flow of hydrochloric acid solution and found measurable interaction with the primary and with the secondary flow structure when the Reynolds and Hartmann moduli were approximately equal and at least of order unity. A significant conclusion of this study is that the one-fluid or continuum model of hydromagnetic flow which assumes no net electrical charge is valid for electrolytes in the absence of large gradients.

3. EXPERIMENTAL TECHNIQUES AND APPARATUS

In order to achieve the objectives of this investigation most expeditiously, flow visualization (including motion-picture photography) was employed to permit observation of the transition phenomenon as

influenced by the magnetic field and to make possible quantitative determination of tangential velocity without the need for insertion of probes. A concentrated aqueous solution of ammonium chloride (350 g/liter) was selected as the electrically conducting working fluid. Operation was at 94°C, at which temperature the pertinent physical properties of the solution are:

σ, electrical conductivity (mho/cm) = 0.837,

μ, absolute viscosity (poise) = 4.1×10^{-3},

ρ, density (g/cm^3) = 1.041.

The dye employed for flow visualization was a dilute solution of soluble red coal-tar base food color in aqueous NH_4Cl, the concentration of which was adjusted to provide neutral buoyancy of the dye solution in the working fluid under operating conditions.

The 10-cm-diam vortex tube used in most of the experiments described here is illustrated in Fig. 2. Note that the flow field was generated by injection ghrough 0.0635-cm-wide slits entering precisely tangentially and extending the full 40-cm-length of the tube. Operation with 1, 2, and 4 slits feeding was possible by blocking appropriate slit entrances. A baffled annular jacket which surrounded the tube and through which the working fluid was circulated served to supply fluid to the slits uniformly through a low porosity inner shell which minimized transfer of turbulence from the annulus to the slit inlet. Rapid circulation of fluid through the annulus also served to minimize axial and circumferential temperature gradients which can induce flow instabilities. Fluid which passed through the vortex tube was exhausted

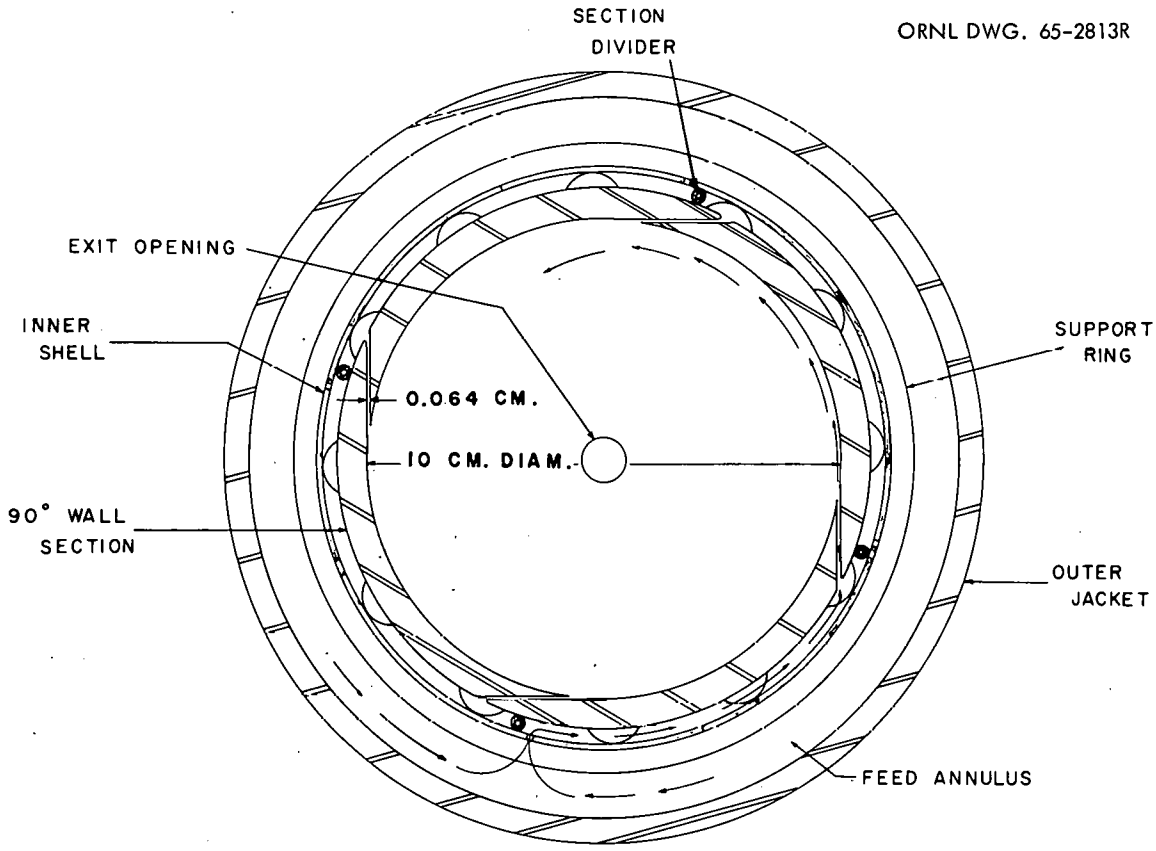

Fig. 2. Slit-Fed Vortex Tube (10-cm diameter x 41-cm long).

at the center of one end by means of a 0.625-cm-diam orifice joined to a long plastic return line to maximize the electrical resistance to ground. This was necessary to minimize the induced radial electric current flow which would interact with the magnetic field to produce flow-retarding body forces. Note that in the absence of radial electric current flow there is no influence of a constant, uniform axial magnetic field on the stationary velocity distribution in two-dimensional vortex flow.† Hence, this flow affords the opportunity for study of the direct influence of the magnetic field on stability.

The tube assembly was fabricated of typer 347 stainless steel (non-magnetic), and was provided with Plexiglas end walls to enable flow visualization. As in the earlier work with the 2.8-cm-diam tubes, observation of dye filaments injected into the boundary layer along the concave wall at several circumferential positions near the mid-axial plane was the primary technique for determining the influence of the magnetic field on flow statbility. Dye injection positions in the end wall opposite the discharge opening were provided to make possible the study of flow in the end-wall boundary layer. Tangential velocities were determined by measuring the time required for a small dye "puff" to complete one or two revolutions at a measured reference radius. Since the reference radius varied slightly from measurement to measurement, all velocities were corrected to a radius ratio of 0.8 by assuming a free vortex velocity profile ($q_\theta \sim 1/r$) over the radius range of interest. The uncertainty introduced by this assumption is not considered to be serious.

---

†See "Jet-Injection Boundary-Layer Profile" – Section 5.

The internal dimensions of the vortex chamber (10 cm × 40 cm) were chosen to maximize utilization of the working volume of the largest air-core solenoid available in the Oak Ridge National Laboratory Magnet Laboratory. The tube was installed with its axis coincident with that of the solenoid, as indicated in Fig. 3 which depicts schematically the all stainless steel (300 series) system for recirculating the working fluid. This water-cooled copper magnet has a working bore of 16.5 cm and a length of about 58 cm and develops a peak field of 75 kgauss with a dc power input of about 6.5 Mw. The field is uniform to within ±1% over the 5 cm tube radius, falling off to about 85% of the peak intensity at the ends of the 40-cm chamber. The maximum Hartmann modulus (based on tube radius) which could be attained in these experiments is 172 as compared with 42 in the earlier work.[6-7] Since the Hartmann modulus determines the magnitude of the magnetic stabilization effect, the new experiments have enabled extension of the measurements to much higher values of the critical tangential Reynolds modulus.

4. EXPERIMENTAL RESULTS

Flow Visualization

As has been indicated, primary emphasis in these experiments was on observation of the effect of an axial magnetic field on the transition from a stable, laminar flow to a time-dependent flow which ultimately becomes turbulent. This transition phenomenon is too complex to describe adequately, but certain consistently observed

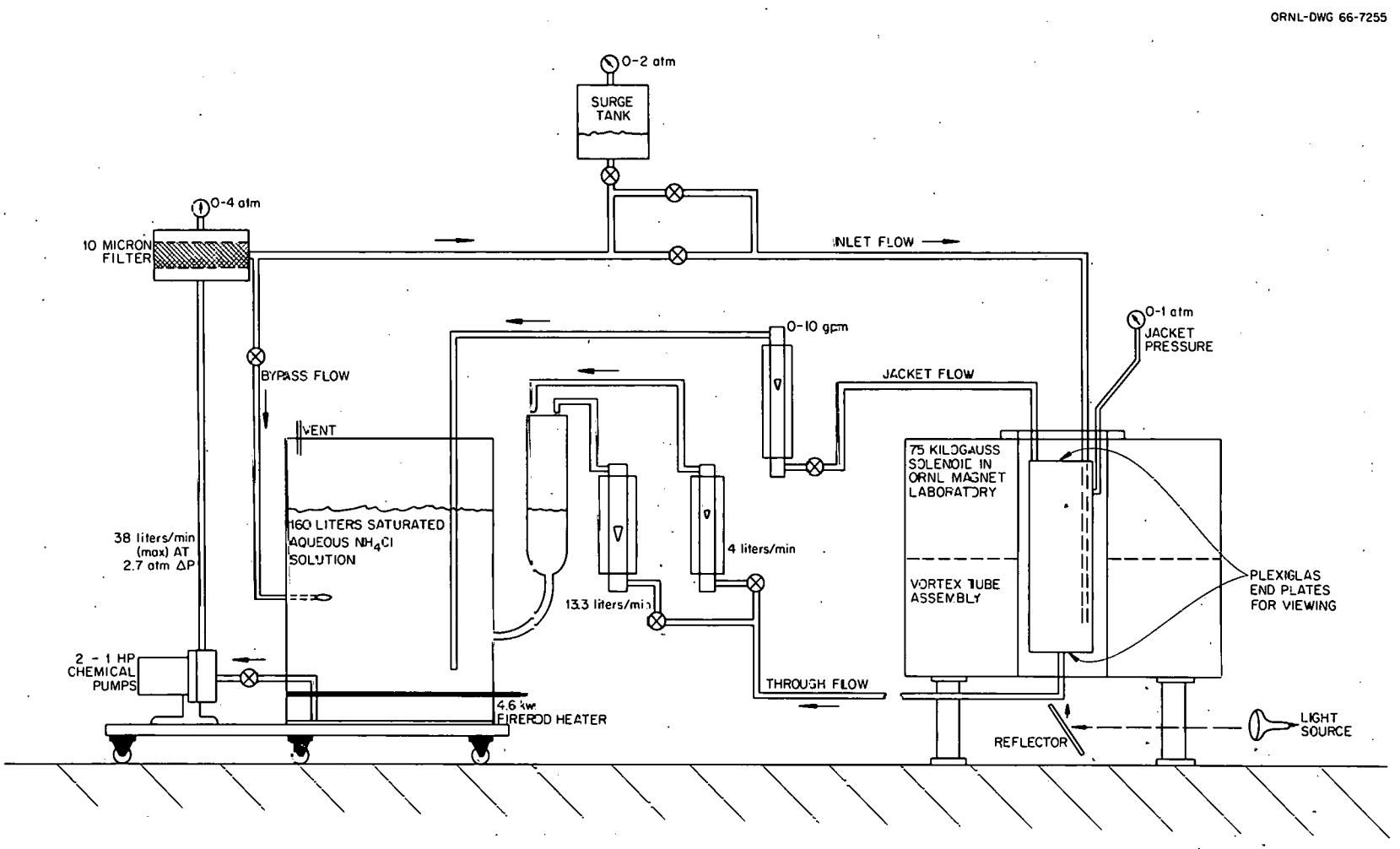

Fig. 3. Schematic Flow Diagram.

features are worthy of note.† When the flow was laminar, dye introduced through the concave wall into the boundary layer (or alternatively introduced tangentially through a feed slit) followed the streamlines which spiral radially inward near the periphery, where the flow was approximately two dimensional, and picked up an increasing axial component as the tube center was approached. No reverse (i.e., upward) flow was noted except near the solid end wall.

When the tangential Reynolds modulus exceeded a critical value which depends on the number of slits injecting fluid and on the strength of the magnetic field, the initial evidence of transition was a periodic swelling of the dye trace near the concave wall just upstream from a driving slit. The periodicity of the instability was verified by measurements of instantaneous surface heat flux using a hot-film sensor (gold film deposited on an epoxy resin plug contoured to fit flush with the inside tube surface and operated at constant temperature as described in Ref. 14), as well as with a constant current hot-film anemometer probe positioned near the surface.

No regular, cell-like structure was observed in the secondary flow at transition. In the Taylor instability of flow between concentric rotating cylinders[15] and in the Görtler instability of flow along a concave wall immersed in a uniform free stream,[16] the secondary flow is stationary in nature and exhibits the form of counterrotating cellular vortices whose axes are parallel to the basic flow direction. Although these cellular vortices were not observed at the transition point in the present experiments, it is nevertheless possible that the Taylor-Görtler mechanism may be responsible for the transition. The

†The observations are based on the two-dimensional impression obtained by viewing along the tube axis through the transparent end walls; hence, important details of the flow may elude the observer.

apparent periodicity could result, for example, from even very slow axial convection of a stationary disturbance past the fixed point of reference; furthemore, the influence of the jets in disturbing the flow near the wall might prevent formation of recognizable Taylor vortices.

When the tangential Reynolds modulus was increased a percent or two above the point corresponding to the first observation of transition, the dye trace in the vicinity of the wall and upstream of a slit exhibited a slow oscillation (period approximagely equal to the time required for the dye to move from one slit to the next). This, of course, appeared as a radial displacement in the two-dimensional view. Irregular rolling of the dye trace around a circumferential axis was also observed when the transition Reynolds modulus was exceeded by at least several percent. This might be interpreted as evidence of the existence of Taylor-Görtler cells, but there was certainly no well-defined pattern observable. The amplitude of the oscillation increased with further increase in tangential Reynolds modulus until, when the Reynolds modulus was 5% or more above transition, the dye trace distorted under the influence of the gradient in tangential velocity into three-dimesnional vortex loops reminiscent of those identified by Hama et al.[17] during transition induced by a trip wire in a boundary layer on a flat plate. Note, however, that the initial instability on a flat plate was two dimensional, as contrasted with the three-dimensional instability associated with flow on a curved surface. Breakup of the dye trace correlates with the appearance of increasing randomness in the signals from both the hot-film surface sensor and the anemometer, and it was concluded that the flow was becoming turbulent. It should be pointed out

that the Reynolds modulus at transition was reproducible to within a few percent when the transition point was approached from either below or above and was not significantly dependent on the rate at which the point was approached. Similar results obtained in Taylor and Taylor-Görtler instability experiments suggest, again, that the same mechanism may be involved.

When transition occurred under the influence of an axial magnetic field, there was no significant effect on the qualitative observations just described. This is to say that the basic hydrodynamic character of the instability did not appear to be altered by the magnetic field.† However, the field did effect a reduction in amplitude of the oscillations when the tangential Reynolds modulus was above the value corresponding to transition, as will be discussed.

Figure 4 depicts the development of a three-dimensional "vortex loop" for the case in which there is no magnetic field and the tangential Reynolds modulus (based on tube radius and the measured tangential velocity at a radius ratio of 0.8) is 3190 (as compared with a critical Reynolds modulus for this case of about 500).†† Hence, Fig. 4 illustrates the fully developed instability, not the transition phenomenon. Note that there are two slits feeding, one entering at the five o'clock position through which the dye also enters; and the other, at eleven o'clock. Rotation is clockwise. Flow spirals radially inward and is removed at the center of one end. The dark region is a shadow of the exit opening, tube, and clamp. In frame 1 the dye trace is seen to emerge from the slit and to follow the wall

---

†The magnetic Reynolds modulus is very small for these experiments.

††Figures 4 through 7 are reproductions of 16-mm motion pictures; the complete film is available on loan from the Oak Ridge National Laboratory.

PHOTO 72360

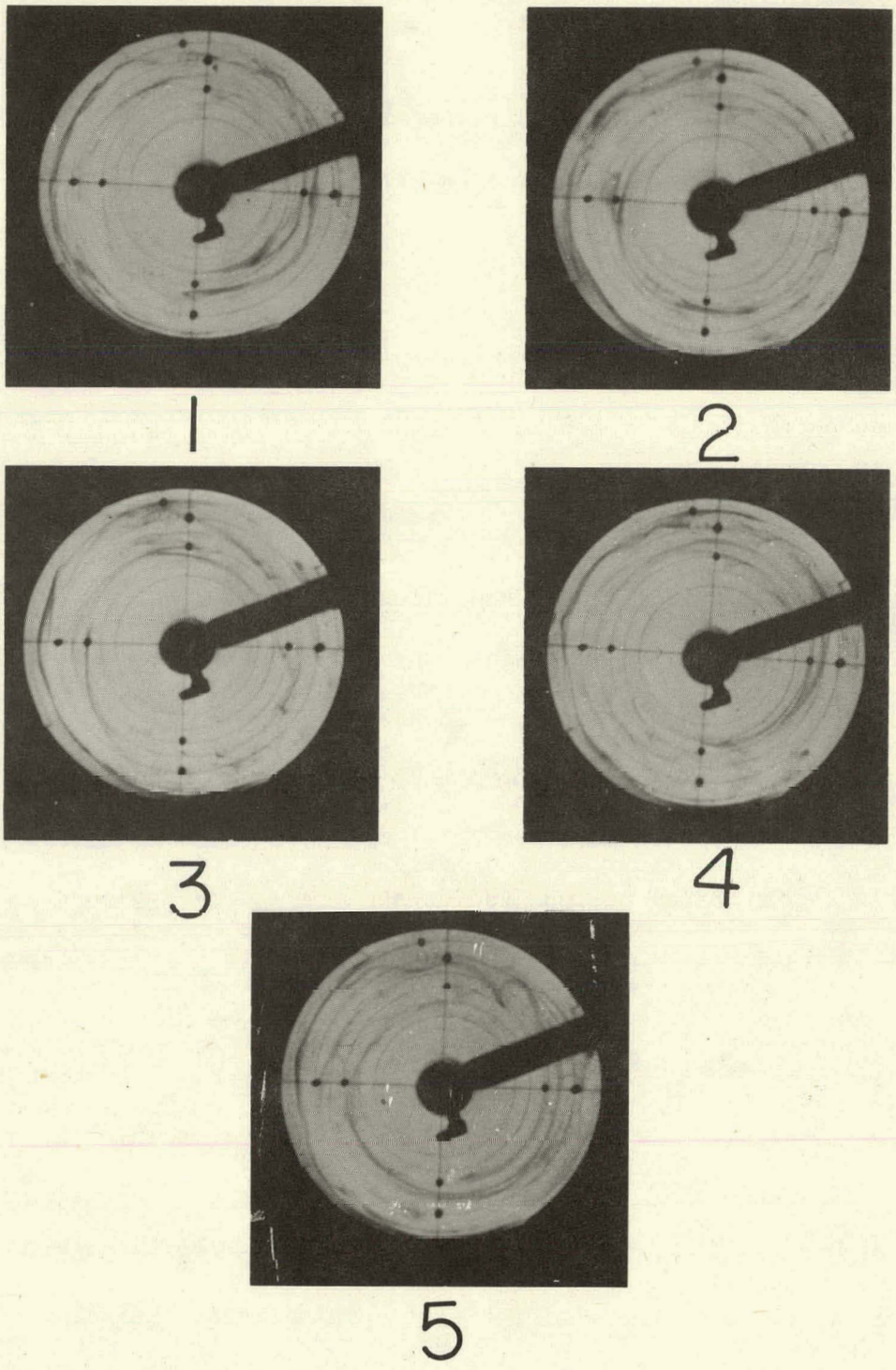

Fig. 4. Development of a "Vortex Loop" in Unstable Jet-Driven Vortex Flow. $N_{Re\,\theta} = 3190$; $N_{Ha} = 0$ (clockwise rotation – jets at five o'clock and eleven o'clock with dye injection at five o'clock).

contour closely for an angular distance of about 90 deg (i.e., halfway between slits). In frame 2, the trace separates from the wall 60 deg from the slit. In frames 3 and 4, the dye trace continues to follow the general curvature of the wall for about 180 deg, but sinusoidal waves form which are actually three dimensional and which appear to amplify in the vicinity of the next injection slit (180 deg downstream). In frame 5, the disturbance has been convected radially inward, amplified further, and under the influence of the tangential velocity gradient distorted into a loop (one o'clock position) which is observed to be three dimensional. Note that the emerging dye trace is again attached to the wall for about 90 deg. Analysis of these photographs suggests that the interaction of the jets with the boundary-layer flow may significantly distort the Taylor-Görtler mechanism, if indeed the latter does play a significant role, so as to make any interpretation uncertain. For example, rapid deceleration of the jet by the action of wall shear may result in local "separation" of the fluid from the wall under the influence of the radial pressure gradient induced by the mean tangential motion [Fig. 4 (2)].

Magnetic Stabilization

Large-amplitude velocity fluctuations, as can be observed in Fig. 4, suggest gross eddy mixing which would make quantitative molecular separation as desired for the applications unlikely. That the magnetic field does indeed inhibit transition to an unstable flow is exhibited in Fig. 5, where again an axial view is presented of the 10-cm-diam tube operating with two slits. The flow is clockwise with

PHOTO 72357

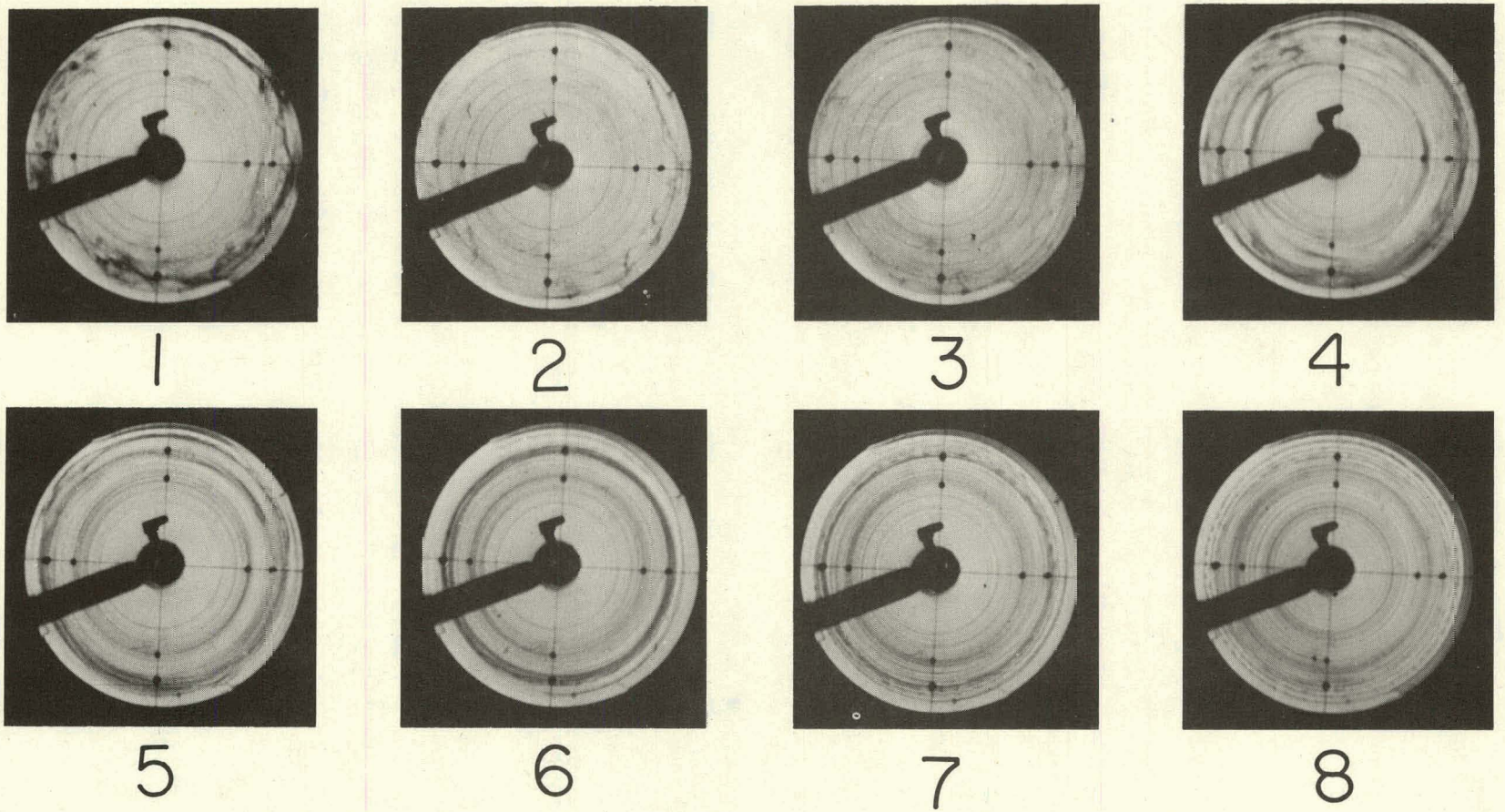

Fig. 5. Stabilization of Jet-Driven Vortex Flow by an Axial Magnetic Field. N_{Re_ϑ} = 6600; N_{Ha} increasing from 0 (Frame 1) to 172 (Frame 8) [clockwise rotation – jets at five c'clock and eleven o'clock with dye injection at eleven o'clock].

the slits at eleven o'clock (dye injection position) and five o'clock. The characteristic tangential Reynolds modulus is 6600 for all of these frames. With no applied field corresponding to frame 1 at the upper left, the instability is made evident by large-scale fluctuations in the dye trace, essentially complete disorganization of the flow pattern, and strong radial mixing. In successive sequences (2) through (8), the magnetic field is increased in approximagely 10 kilogauss increments keeping the Reynolds modulus constant. The first definite evidence of a stabilizing effect is the appearance of laminar dye rings near the axis of the tube at approximately 20 kilogauss (3), indicating that the flow field stabilizes first in the interior. As the field increases, the laminar rings increase in radius and the outer portion of the flow ultimately stabilizes. At the full field 75 kilogauss (Hartmann modulus 172), the macroscopic flow is completely stable (8). The only disturbance which is not eliminated is the very small-scale ripple associated with vortex-street formation at the lips of the injection slits.

When the magnetic field is slowly decreased, breakdown of the laminar flow is observed to occur first near the wall, the unstable region spreading to the center of the tube as the field approaches zero. Further evidence that the interior region of the flow is more readily stabilized than that near the periphery is presented in Fig. 6. Here the tangential Reynolds modulus is 13,200 as compared with the maximum value of 7600 for complete stabilization throughout the flow field under the influence of the full magnetic field. Note that in

PHOTO 72361

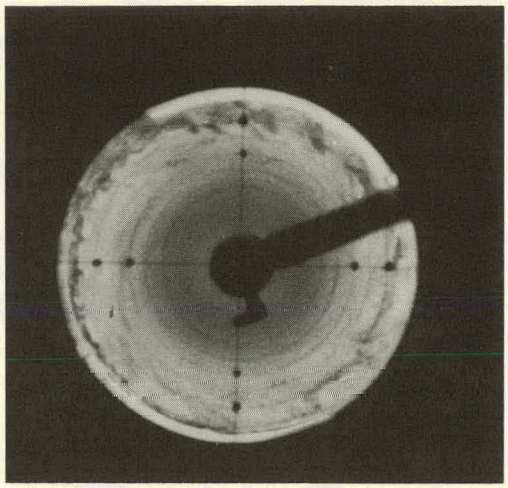

1

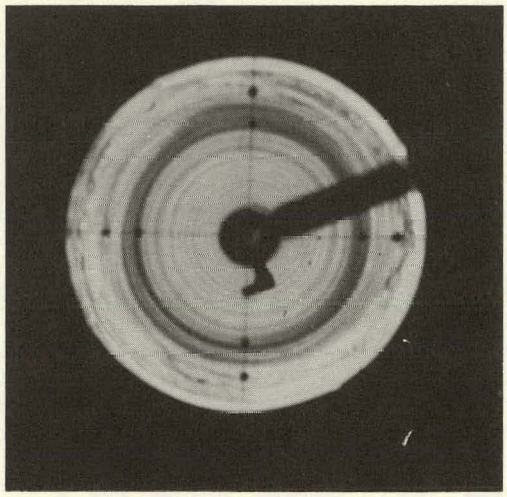

2

Fig. 6. Stabilizing Effect of an Axial Magnetic Field on Jet-Driven Vortex Flow — Tangential Reynolds Modulus Above the Critical Value. $N_{Re\,\theta}$ = 13,200. Frame 1: N_{Ha} = 0; Frame 2: N_{Ha} = 172 (clockwise rotation — jets at five o'clock and eleven o'clock with dye injection at five o'clock).

frame 1 for the case in which there is no magnetic field, essentially complete turbulent mixing is evident in the interior by the uniform dye coloration; with the 75 kilogauss field (frame 2), we see that while the outer region of the flow remains turbulent, laminar flow is evidenced in the interior by the formation of a stable spiral ring structure. Similar results were observed at a Reynolds modulus of 26,000. This is important because in the applications the critical Reynolds modulus may be above that corresponding to complete stabilization with the maximum feasible magnetic field. Nevertheless, the interior fuel region may be stabilized sufficiently to permit adequate fuel retention.

In Fig. 7 the influence of the full magnetic field on flow near the concave wall at a Reynolds modulus above the critical value is revealed. It is seen that the amplitude of the disturbance is decreased (by as much as a factor of 4), and the wave length likewise decreased by the magnetic interaction.

Data and Correlations

Stabilization

Careful determinations were made of the critical Reynolds modulus at transition to instability in the boundary layer on the concave wall, using the dye-pulse injection method. The experimental results are summarized in Fig. 8 in which the critical Reynolds modulus, $N^{*}_{Re_\theta}$ (based on the tube radius r_o, and the tangential velocity, $V_{0.8}$ at a radius of $0.8\ r_o$), is plotted as a function of Hartmann modulus N_{Ha}:

PHOTO 72362

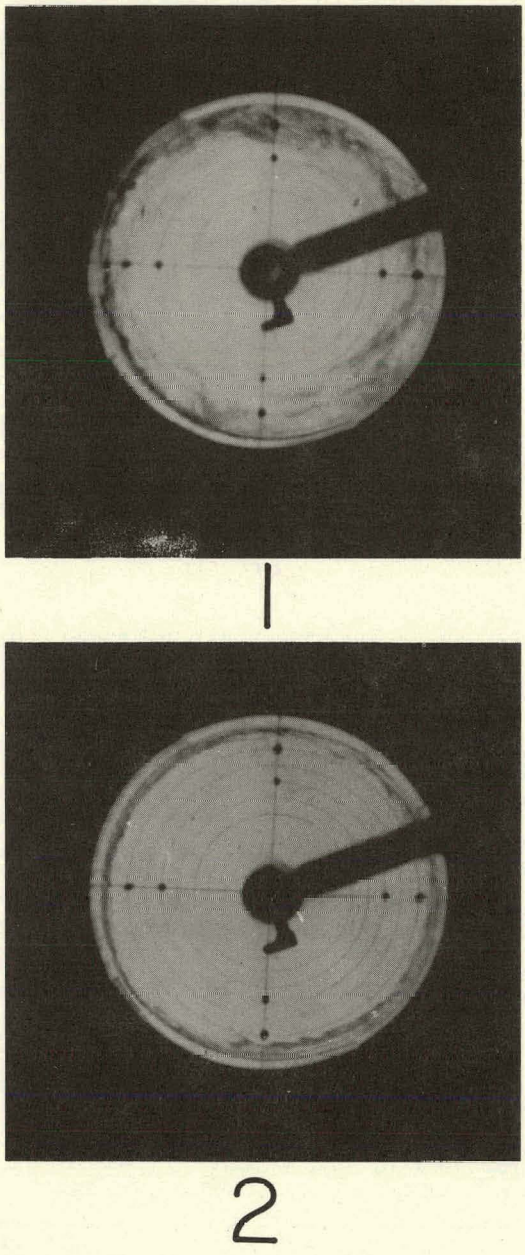

Fig. 7. Effect of an Axial Magnetic Field on Jet-Driven Vortex Flow Near the Concave Wall When the Tangential Reynolds Modulus is Above the Critical Value. $N_{Re\theta}$ = 13,200. Frame 1: N_{Ha} = 0; Frame 2: N_{Ha} = 172 (clockwise rotation — jets at five o'clock and eleven o'clock with dye injection at five o'clock).

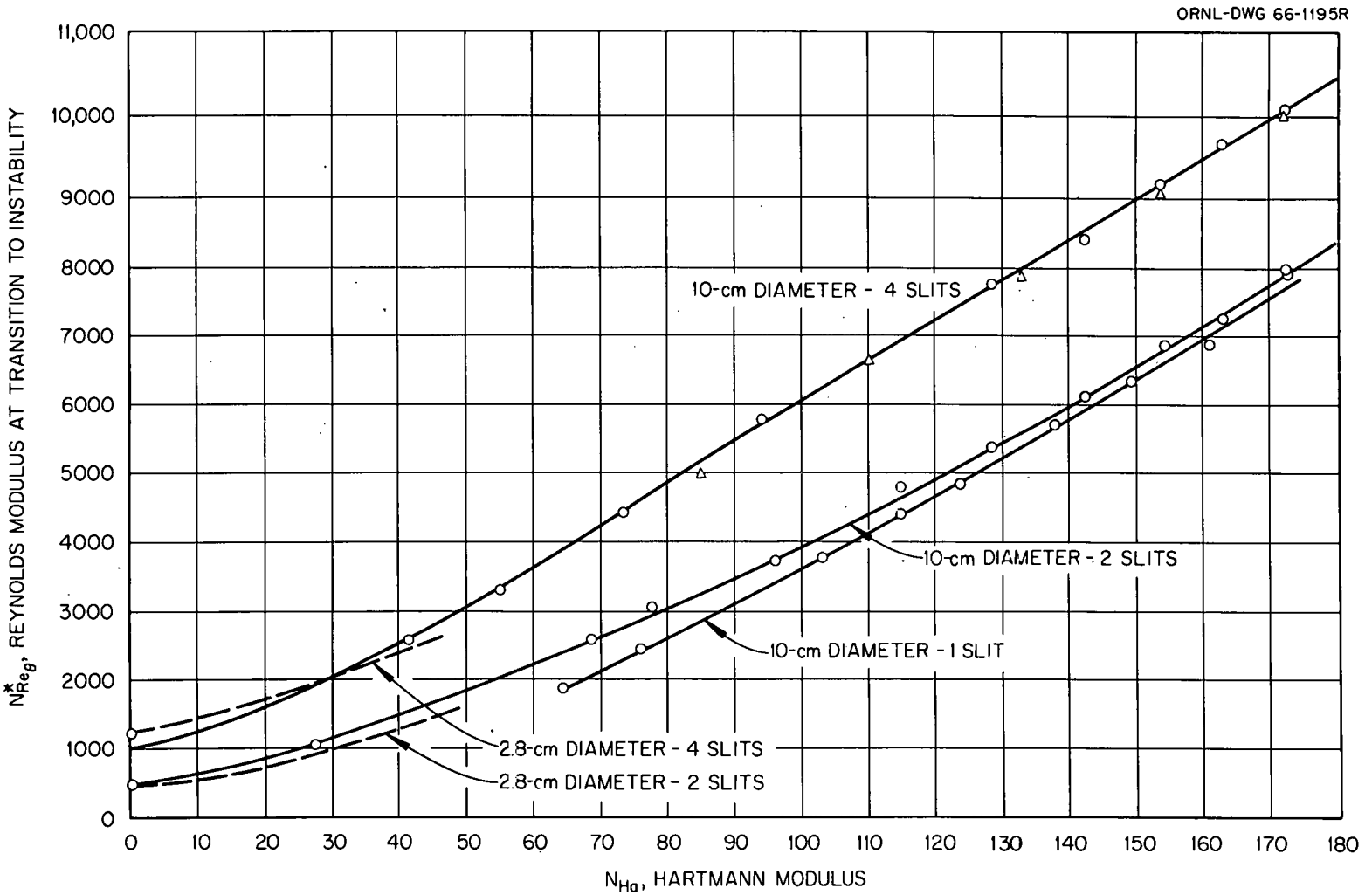

Fig. 8. Summary of Hydromagnetic Stabilization Experiments with 2.8- and 10-cm-diam Jet-Driven Vortex Tubes (Reynolds modulus versus Hartmann modulus).

$$N_{Ha} \equiv \sqrt{\sigma/\mu}\ B_0\ r_o \quad ,$$

where σ is the electrical conductivity, μ is the absolute viscosity, and B_0 the magnitude of the applied magnetic induction vector (assumed to be parallel to the axis of the vortex tube). The Hartmann modulus, which is proportional to the square root of the ratio of magnetic to viscous forces, has been found to characterize the stability of axisymmetric Couette flow as discussed in Section 2. Note that for the 10-cm-diam tube, increasing N_{Ha} from 0 to the maximum value of 172 (corresponding to B_0 = 75 kgauss), increases $N^*_{Re_\theta}$ from 1200 to about 10,000 for the case of 4 slits, and from 500 to about 8,000 for the case of 2 slits. No stable flow condition could be found for $N_{Ha} < 60$ with only 1-slit feeding; the results for 1- and 2-slit operation are relatively close for $N_{Ha} > 100$. Thermal convection was found to limit stability at very low values of the Reynolds modulus.

The nominal radial Reynolds modulus, N_{Re_r} ($= m/2\ \pi\ \mu$, where m is the total mass throughflow rate per unit tube length) ranged as follows for the three cases:

$$\text{1 slit:}\quad 10.6 \leq N_{Re_r} \leq 32.2 \quad ,$$

$$\text{2 slit:}\quad 16.9 \leq N_{Re_r} \leq 51.3 \quad , \text{ and}$$

$$\text{4 slit:}\quad 23.3 \leq N_{Re_r} \leq 110.5 \quad .$$

The dashed curves at the lower left of the plot represent results of earlier hydromagnetic stabilization experiments;[6,7] agreement with the 10-cm-tube data is fair.

While a plot of the critical tangential Reynolds modulus versus Hartmann modulus (where both moduli are based on the tube radius) is useful for direct comparison of experimental results, it fails to take into account the boundary-layer nature of the flow between jets and is therefore of limited value as a general correlation. That is, growth of the boundary layer downstream from a jet is presumed to be the principle criterion governing the stability of the flow; hence, consideration of the data in terms of moduli appropriate to the boundary layer might produce a useful correlation. Assuming an analogy with the Görtler instability problem in ordinary fluid mechanics (although the experimental observations are not at all conclusive in this regard as has been emphasized), the "Görtler modulus" is here defined in terms of the momentum thickness, Δ, of the boundary layer as

$$N_{G\ddot{o}} \equiv (V_{0.8}\, \Delta/\nu)(\Delta/r_o)^{1/2}$$

where ν is the kinematic viscosity. Note that $V_{0.8}\, \Delta/\nu$ is the tangential Reynolds modulus based on the momentum thickness of the boundary layer. The Hartmann modulus, based on momentum thickness, is defined as follows:

$$N_{Ha_\Delta} \equiv \sqrt{\sigma/\mu}\, B_0\, \Delta \quad .$$

In order to determine Δ, it is assumed that the boundary-layer growth well downstream from a slit is given, to a first approximation,

by the result for a flat plate immersed in a uniform free stream as obtained by the application of boundary-layer theory:[18]

$$\Delta \cong \frac{0.664}{(V_{0.8}/\nu \ell)^{1/2}} \quad ,$$

where ℓ is the circumferential distance between slits and the free stream velocity is taken as $V_{0.8}$. In terms of the tangential Reynolds modulus and number of slits, n, using

$$\ell = 2\pi r_o/n \quad :$$

$$\frac{\Delta}{r_o} = \frac{0.664}{\left(n\, N_{Re_\theta}/2\pi\right)^{1/2}} \quad .$$

The Görtler modulus may now be written:

$$N_{G\ddot{o}} = 0.542\, (2\pi/n)^{3/4}\, (N_{Re_\theta})^{1/4} \quad .$$

Likewise the Hartmann modulus (based on momentum thickness) may be written:

$$N_{Ha_\Delta} = \frac{0.664(2\pi/n)^{1/2}\, N_{Ha}}{(N_{Re_\theta})^{1/2}} \quad .$$

A comparison of the experimental hydromagnetic stability data for the 10-cm-tube in terms of the Görtler modulus at transition to instability (critical Görtler modulus, $N^*_{G\ddot{o}}$) and the Hartmann

modulus (based on momentum thickness) is presented in Fig. 9. Here a fair degree of correlation of the data is evident. The standard error of fit for the fourth degree least-squares curve based on data for 1-, 2-, and 4-slit operation taken collectively is 0.043, considering N_{Ha_Δ} as the dependent variable.[19] Upon close examination, however, it is seen that the individual data points fall on three distinct curves of somewhat lower slope than that of the fourth degree curve. As discussed in Section 5, there is uncertainty as to the validity of the boundary-layer approximation upon which the Görtler and Hartmann moduli are based for conditions corresponding to much of the experimental data. This could account for the observed discrepancies in the results for the three slit numbers even though the Taylor-Görtler mechanism is valid.†

The lower curve in Fig. 9 is based on a stability analysis employing laminar boundary-layer theory, the details of which are described in Section 5.†† Possible explanations for the poor agreement between theory and experiment are also discussed.

In order to improve the data correlation, the exponent of the ratio Δ/r_o in the expression defining the Görtler modulus was modified to yield the lowest standard error of fit. The resulting exponent turned out to be 0.43 as compared with 0.5 based on the Görtler analysis. Figure 10 depicts the resulting correlation of the modulus

$$\left(V^*_{0.8}\,\Delta/\nu\right)\left(\Delta/r_o\right)^{0.43} ,$$

---

†No improvement in the correlation resulted from the use of the theoretical boundary-layer velocity profile well downstream from a jet, as determined in Section 5.

††As discussed in Section 5, the theoretical curve is for the narrow-gap, conducting wall case with $\bar{W} = 0.6$.

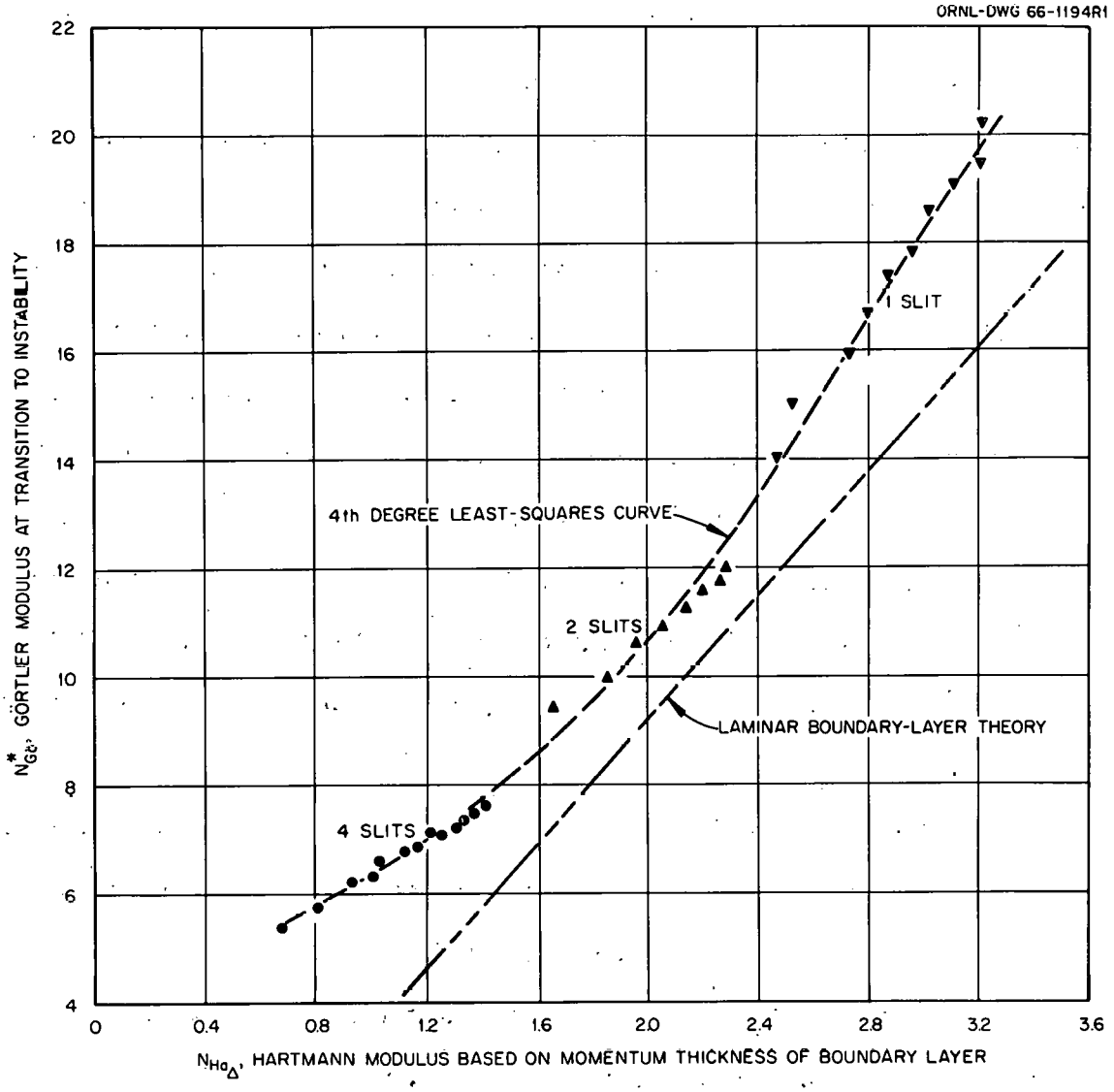

Fig. 9. Summary of Hydromagnetic Stabilization Experiments with a 10-cm-diam Jet-Driven Vortex Tube (Görtler Modulus versus Hartmann Modulus).

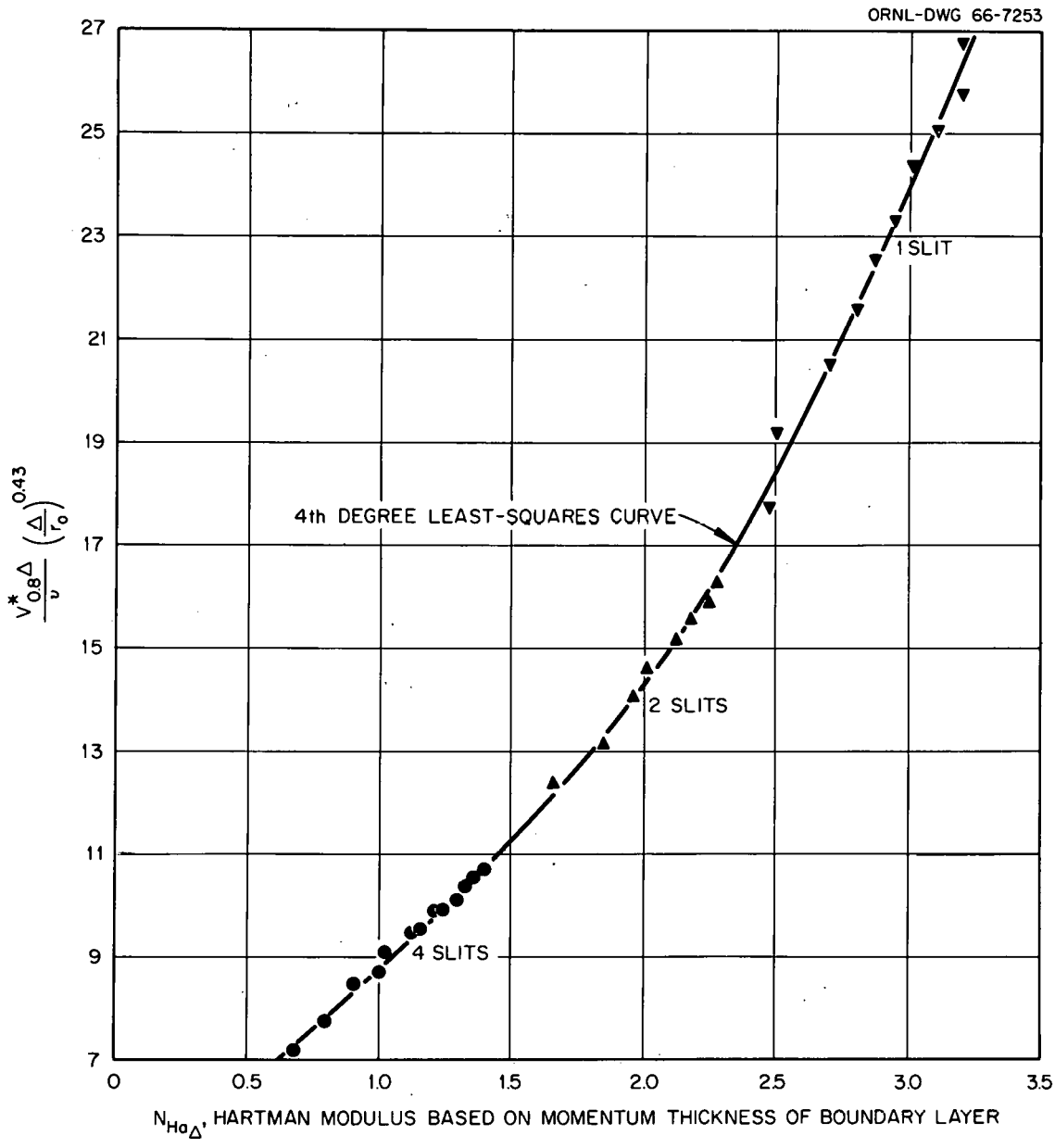

Fig. 10. Summary of Hydromagnetic Stabilization Experiments with a 10-cm-diam Jet-Driven Vortex Tube [Empirical Modulus, $(V^*_{0.8}\,\Delta/\nu)(\Delta/r_o)^{0.43}$ at Transition to Instability versus Hartmann Modulus].

at transition versus the Hartmann modulus (based on momentum thickness). It is seen that the individual data for 1-, 2-, and 4-slit operation fall closely along the 4th degree least-squares curves based on all the data, the standard error of fit being 0.027 with N_{Ha_Δ} considered as the dependent variable. Of course, there is no theoretical justification for an exponenent other than 0.5; but the empirical correlation should be more accurate for interpolation and extrapolation than that based on the theoretically derived Görtler modulus employed in Fig. 9.

Jet Velocity Recovery

An important parameter characterizing the efficiency of vortex generation is the ratio of the tangential velocity to the jet injection velocity. The recovery ratio, $\alpha_{1.0}$, is defined here as the ratio of the tangential velocity (extrapolated to the wall assuming free vortex flow) to the average jet velocity:

$$\alpha_{1.0} = 0.8\, V_{0.8}/V_j \quad ,$$

where V_j is the average jet velocity. From laminar boundary-layer theory as developed in the next Section, it can be shown that, for the case of tangential injection by means of two-dimensional slits (10-cm vortex tube), the recovery ratio depends on the dimensionless jet width parameter, $\overline{W}$:

$$\overline{W} = \frac{N_{Re_r}}{(n\, N_{Re_j}/2\pi)^{1/2}} \quad ,$$

where

$$N_{Re_j} \equiv V_j \, r_o/\nu \quad .$$

In Fig. 11 experimental determinations of $\alpha_{1.0}$ are compared with the theoretical results in terms of the dimensionless jet-width parameter, $\overline{W}$. For the case of magnetic stabilization with the 10-cm tube, agreement to within ±5% is evidence that the theory is satisfactory. Note further that when there is no magnetic stabilization and the flow is no longer laminar, the measured values of $\alpha_{1.0}$ decreased by about 30%, due probably to the increased wall shear induced by turbulence.

Data are also included in Fig. 11 for the case of stabilized vortex flow generated in a 2.8-cm-diam tube by injection through 880 round nozzles, 0.050-cm-diam and arranged in eight rows.[7] The nozzles were directed so that their centerline was tangent to a circle of radius $0.9\ r_o$. Significantly higher recovery ratios were observed for the round jets than for tangential slits when compared on the basis of the parameter $\overline{W}$. This is to be expected, however, since injecting fluid away from the wall should reduce the velocity gradient at the wall and, thereby, reduce the wall shear. From the point of view of maximum recovery, therefore, round nozzles with off-tangent entry are preferred. However, as discussed in Ref. 7, the critical Reynolds modulus for vortex generation by eight rows of round jets is appreciably lower than that for generation by eight slits, the round-jet results being comparable to the two-slit results. Thus, the advantage in recovery ratio gained by the use of round jets is offset by the reduced stability of the flow, and it is not certain that round jets would be more desirable than slits for the applications.

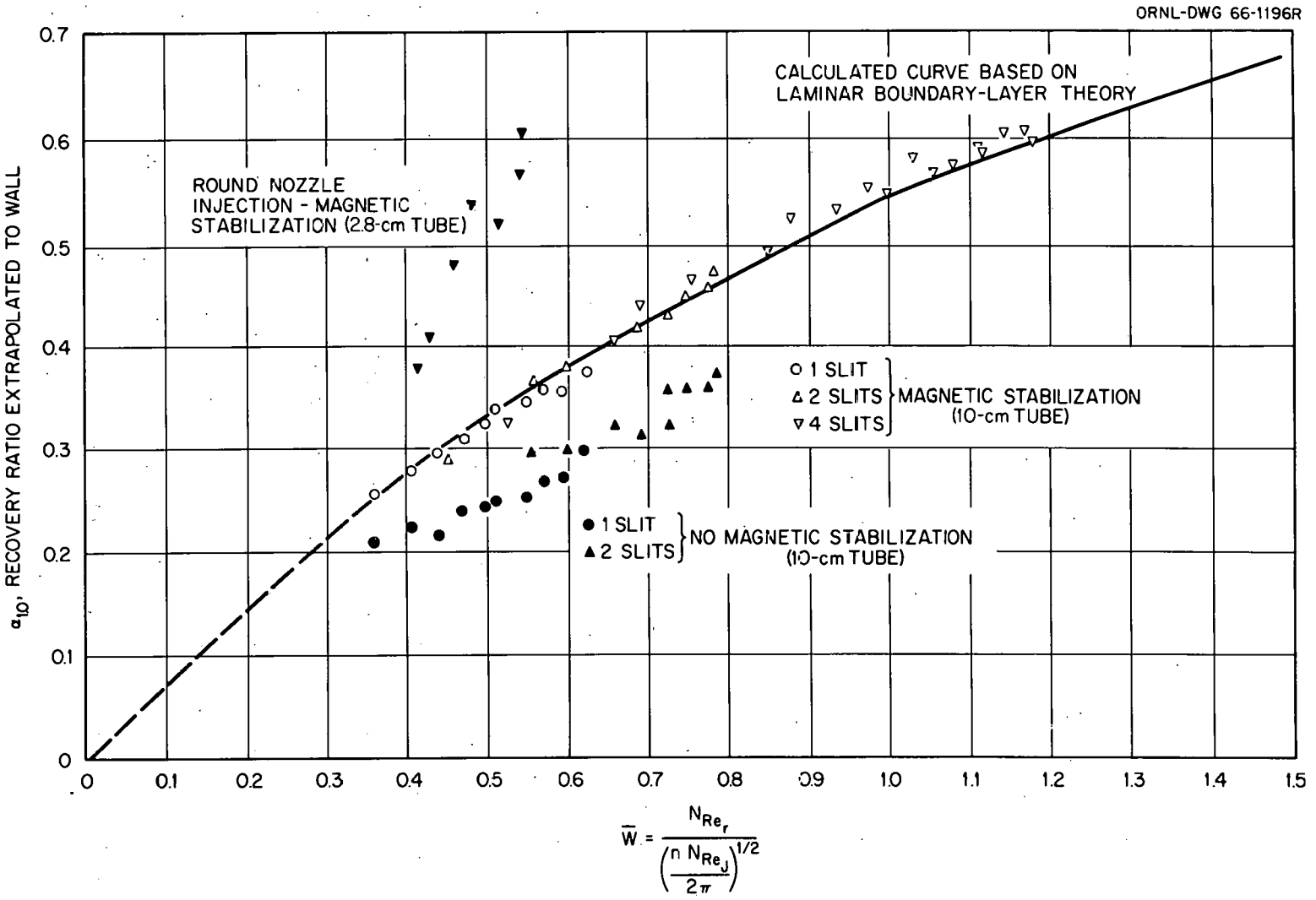

Fig. 11. Correlation of Jet Velocity Recovery Ratio for Magnetically Stabilized and Unstabilized Vortex Flow.

5. ANALYSIS

General Theory

An MHD Görtler-type of stability analysis based on a tangential jet-injection velocity profile over a concave wall has been considered. The stationary jet-injection velocity profile is calculated according to the classical theory of laminar boundary-layer flow. The stability analysis is carried out numerically based on the linear perturbation theory for the jet-injection profile under the influence of an externally applied magnetic field. The fluid is assumed to be incompressible, viscous, and electrically conducting.

Consider a two-dimensional, stationary velocity profile of the form

$$U = U(r,\theta) \quad , \qquad V = V(r,\theta) \quad , \qquad W = 0 \quad , \tag{1}$$

where (U,V,W) are the cylindrical (r,θ,z) components of the velocity vector. An external magnetic induction field B_o is applied in the axial (z) direction. Based on the classical theory of magnetohydrodynamics, it is not difficult to demonstrate that for perfectly conducting walls, the primary interaction between the magnetic field and the flow field given in Eqs. (1) is small, provided the magnetic Prandtl modulus ($N_{Pr_m} = \sigma \mu_o \nu$) is small, where σ is the electrical conductivity, μ_o is the magnetic permeability, and ν is the kinematic viscosity. Allowing the flow field and the magnetic induction field to be perturbed slightly and inserting the perturbed functions into the basic equations of MHD,[11] the following sets of equations (correct to the zeroth and first order of the perturbations) are obtained.

Zeroth Order Equations:

$$U\frac{\partial U}{\partial r} + V\frac{\partial U}{r\partial\theta} - \frac{V^2}{r} = -\frac{\partial P^*}{\partial r} + \nu\left[\left(D_*D + \frac{\partial^2}{r^2\,\partial\theta^2}\right)U - \frac{2}{r^2}\frac{\partial V}{\partial\theta}\right] ,$$

$$U\frac{\partial V}{\partial r} + V\frac{\partial V}{r\partial\theta} + \frac{UV}{r} = -\frac{\partial P^*}{r\partial\theta} + \nu\left[\left(D_*D + \frac{\partial^2}{r^2\,\partial\theta^2}\right)V + \frac{2}{r^2}\frac{\partial U}{\partial\theta}\right] , \qquad (2)$$

$$\frac{\partial U}{\partial r} + \frac{U}{r} + \frac{\partial V}{r\partial\theta} = 0 ,$$

where

$$P^* = \frac{1}{\rho}\left(P + \frac{B_0^2}{2\,\mu_0}\right) = P^*(r,\theta) , \qquad (3)$$

$$D = \frac{d}{dr} , \qquad D_* = \frac{d}{dr} + \frac{1}{r} , \qquad (4)$$

P is the undisturbed fluid pressure, ρ is the fluid density, and ν is the kinematic viscosity.

First Order Equations:

$$\left(\frac{\partial}{\partial t} + \frac{\partial U}{\partial r} + U\frac{\partial}{\partial r} + V\frac{\partial}{r\partial\theta} - \nu\nabla^2\right)u' + \left(\frac{\partial U}{r\partial\theta} - \frac{2V}{r} + \frac{2\nu}{r^2}\frac{\partial}{\partial\theta}\right)v'$$

$$-\frac{B_0}{\rho\mu_0}\frac{\partial b_r}{\partial z} + \frac{\partial p^*}{\partial r} = 0 , \qquad (5)$$

Continued

$$\left(\frac{\partial V}{\partial r} + \frac{V}{r} - \frac{2\nu}{r^2} \frac{\partial}{\partial \theta} \right) u' + \left(\frac{\partial}{\partial t} + U \frac{\partial}{\partial r} + V \frac{\partial}{r\partial \theta} + \frac{\partial V}{r\partial \theta} + \frac{U}{r} - \nu \nabla^2 \right) v'$$

$$- \frac{B_o}{\rho \mu_o} \frac{\partial b_\theta}{\partial z} + \frac{\partial p^*}{r\partial \theta} = 0 \quad ,$$

$$\left(\frac{\partial}{\partial t} + U \frac{\partial}{\partial r} + V \frac{\partial}{r\partial \theta} - \nu \nabla^2 - \frac{\nu}{r^2} \right) w' - \frac{B_o}{\rho \mu_o} \frac{\partial b_z}{\partial z} + \frac{\partial p^*}{\partial z} = 0 \quad ,$$

$$B_o \frac{\partial u'}{\partial z} - \left(\frac{\partial}{\partial t} + U \frac{\partial}{\partial r} + V \frac{\partial}{r\partial \theta} - \frac{\partial U}{\partial r} - \eta \nabla^2 \right) b_r + \left(\frac{\partial U}{r\partial \theta} - \frac{2\eta}{r^2} \frac{\partial}{\partial \theta} \right) b_\theta = 0 \quad ,$$

$$B_o \frac{\partial v'}{\partial z} + \left(\frac{\partial V}{\partial r} - \frac{V}{r} + \frac{2\eta}{r^2} \frac{\partial}{\partial \theta} \right) b_r$$

$$- \left(\frac{\partial}{\partial t} + U \frac{\partial}{\partial r} + V \frac{\partial}{r\partial \theta} - \frac{\partial V}{r\partial \theta} - \frac{U}{r} - \eta \nabla^2 \right) b_\theta = 0 \quad ,$$

$$B_o \frac{\partial w'}{\partial z} - \left(\frac{\partial}{\partial t} + U \frac{\partial}{\partial r} + V \frac{\partial}{r\partial \theta} - \eta \nabla^2 + \frac{\eta}{r^2} \right) b_z = 0 \quad ,$$

$$\frac{\partial u'}{\partial r} + \frac{u'}{r} + \frac{\partial v'}{r\partial \theta} + \frac{\partial w'}{\partial z} = 0 \quad ,$$

$$\frac{\partial b_r}{\partial r} + \frac{b_r}{r} + \frac{\partial b_\theta}{r\partial \theta} + \frac{\partial b_z}{\partial z} = 0 \quad , \qquad (5)$$

where (u', v', w') are the perturbations of the cylindrical components of the velocity vector, (b_r, b_θ, b_z) are the perturbations of the cylindrical components of the magnetic induction vector, p^* is the perturbation of P^*, $\eta = (\sigma \mu_0)^{-1}$ is the magnetic viscosity, and

$$\nabla^2 = D_* D + \frac{\partial^2}{r^2 \partial \theta^2} + \frac{\partial^2}{\partial z^2} \quad . \tag{6}$$

In the above equations the rationalized MKS system of units is used.

Jet-Injection Boundary-Layer Velocity Profile

As observed experimentally, the primary flow in a jet-driven vortex tube consists of a thin boundary layer near the tube wall in which the influence of the driving jets and frictional wall drag are felt, followed by an interior region in which the flow appears to become nearly axisymmetric and the tangential and radial velocities are approximately inversely proportional to the radial distance r measured from the axis of the vortex. Near the axis, a central core forms in which the radial and tangential velocity decreases and the fluid moves axially toward the exit. We shall ignore the central core containing the axial component of the primary flow entirely, and consider only the outer boundary layer in detail.

Since B_0 is a constant, substitution of Eq. (3) into Eq. (2) gives us the ordinary two-dimensional Navier-Stokes equations in cylindrical coordinates. The primary, or zeroth-order flow is not affected by the applied magnetic field.

It is well known[20] that the two-dimensional boundary-layer equations are unaffected by the curvature of the surface if the boundary-layer thickness is much less than the radius of curvature. Formally, we make the following subsitution in Eq. (2):

$$\bar{Y} = \frac{r_o - r}{\delta} \ ,$$

$$\bar{X} = \frac{r_o \theta}{\ell} \ ,$$

$$\bar{U} = -\frac{U \ell}{V_j \delta} \ ,$$

$$\bar{V} = \frac{V}{V_j} \ , \qquad (7)$$

where ℓ is the distance between jets, measured along the outer tube periphery,

r_o is the tube radius,

V_j is the average jet injection velocity, and

$\delta = \ell / \sqrt{V_j \ell / \nu}$, the boundary-layer thickness parameter which is assumed to be small.

Strictly speaking, $\bar{Y}$ is the normal distance from the wall divided by δ. Immediately downstream of a slit opening, the distance from the wall is not precisely $(r_o - r)$ because a portion of the wall is machined away to make the slit. This difficulty does not affect the boundary-layer calculations, but strictly should be taken into account in

converting the results back into vortex tube velocity profiles, especially for the radial velocity. However, we shall not make use of the velocity just downstream of the jets. Retaining only the lowest-order terms in δ, we obtain the usual dimensionless boundary-layer equations:

$$\bar{U}\frac{\partial \bar{V}}{\partial \bar{Y}} + \bar{V}\frac{\partial \bar{V}}{\partial \bar{X}} = \frac{\partial^2 \bar{V}}{\partial \bar{Y}^2} \quad ,$$

$$\frac{\partial \bar{U}}{\partial \bar{Y}} + \frac{\partial \bar{V}}{\partial \bar{X}} = 0 \quad . \tag{8}$$

The boundary-layer approximations permit us to treat the problem as one in rectangular coordinates, but we cannot ignore the periodicity of the flow in the θ- or $\bar{X}$-direction. In rectangular coordinates, we "unroll" the vortex tube to obtain a series of flat plates separated by tangential injection slits (see sketch in Fig. 12). We consider an infinite number of such plates so that the flow will be periodic. Letting W denote the jet width, we assume

$$W \sim \delta \ll \ell \quad . \tag{9}$$

The velocity profile in the slit exit is assumed to be parabolic.

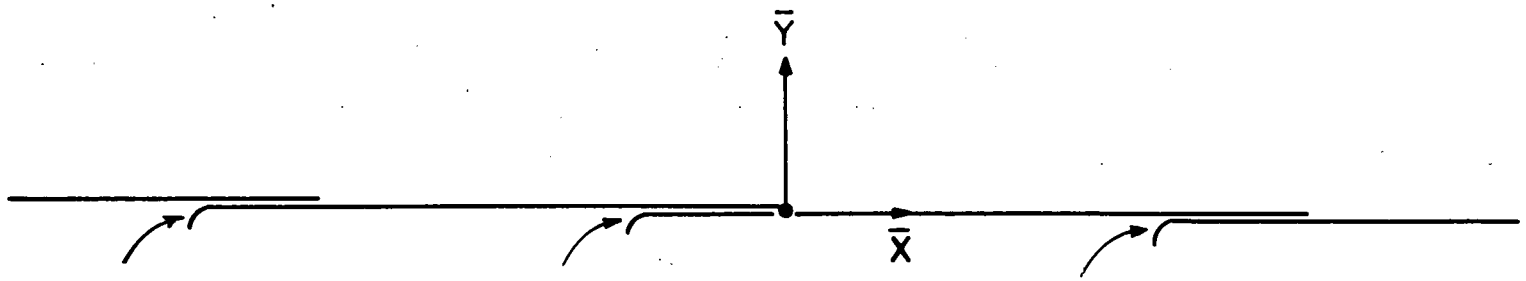

Fig. 12. Jet-Injection Geometries for Calculations.

Boundary Conditions

The boundary conditions for Eq. (8) are

$$\overline{U}(\overline{X},0) = 0 \quad ,$$

$$\overline{V}(\overline{X},0) = 0 \quad ,$$

$$\frac{\partial \overline{V}}{\partial \overline{Y}} \to 0 \text{ as } \overline{Y} \to \infty \quad ,$$

$$\overline{V}(0,\overline{Y}) = \begin{cases} \overline{V}(1,\overline{Y} - \overline{W}) \quad , & \overline{Y} > \overline{W} \quad , \\ \dfrac{6\ \overline{Y}(\overline{W} - \overline{Y})}{\overline{W}^2} \quad , & \overline{Y} < \overline{W} \quad , \end{cases} \tag{10}$$

where $\overline{W} = W/\delta = (W/\ell)\sqrt{V_j \ell/\nu}$ is the dimensionless jet-width.

The system of equations, (8) and (10), contains only the single parameter $\overline{W}$. Hence the solution, and in particular

$$\alpha_{1.0} \equiv \lim_{\overline{Y} \to \infty} \overline{V} \quad , \tag{11}$$

which we call the recovery ratio, should be uniquely determined by $\overline{W}$. In a jet-driven vortex tube $\overline{W}$ can be rewritten in terms of the radial Reynolds modulus, N_{Re_r}, the tangential jet Reynolds modulus, N_{Re_j}, and the number of jets, n, as

$$\overline{W} = \frac{N_{Re_r}}{(n\ N_{Re_j}/2\pi)^{1/2}} \quad . \tag{12}$$

Calculation of Jet Profiles

The solution of the Eqs. (8) and (10) was carried out by means of a finite-difference technique of the explicit, forward-marching type. The difference approximation was of second-order accuracy in the $\overline{Y}$ mesh size, and first-order in the $\overline{X}$ mesh size.

The last boundary condition of Eqs. (10) involves values of the velocity at both ends of the interval and prevents the direct use of a marching-type solution. This difficulty was avoided by using an iteration method involving a sequence of marching problems with

$$\overline{V}^{o}(1,\overline{Y}) = \text{arbitrary constant} \quad ,$$

$$\overline{V}^{k+1}(0,\overline{Y}) = \begin{cases} \overline{V}^{k}(1,\overline{Y}-\overline{W}) & , \ \overline{Y} > \overline{W} \\ 6\,\overline{Y}(\overline{W}-\overline{Y})/\overline{W}^{2} & , \ \overline{Y} < \overline{W} \end{cases} \tag{13}$$

The sequence was continued until adequate convergence was obtained. The result was independent of $\overline{V}^{o}$.

The boundary condition $\partial\overline{V}/\partial\overline{Y} \to 0$ of Eqs. (10) was actually applied at a finite value of $\overline{Y}$, $\overline{Y}_{max}$, which was chosen arbitrarily but large enough to be outside of the boundary layer. The value of $\overline{Y}_{max}$ varied from 7 to 15 in the cases run.

The number of $\overline{Y}$ mesh points varied from 60 to 100. The minimum number of $\overline{Y}$ mesh points across the jet itself was about six and was probably a limiting factor in accuracy. The size of the $\overline{X}$ increment was determined by numerical stability requirements. The resulting number of $\overline{X}$ mesh points varied from several thousand to about a

hundred thousand. The parameter $\overline{W}$ was varied from 0.4 to 3.0. Computer time (CDC 1604) varied strongly with $\overline{W}$ from several minutes with W = 3.0 to several hours with $\overline{W}$ = 0.4. (The use of an implicit difference technique would clearly be desirable for small values of $\overline{W}$.)

No accurate estimate was made of the error resulting from the choice of mesh size and $\overline{Y}_{max}$ used. Errors on the order of 5 to 10% seem likely. The only experimental quantity available for comparison is the recovery ratio, $\alpha_{1.0}$; i.e., the ratio of tangential velocity beyond the boundary layer (corrected for tube curvature) to the average jet velocity. Comparison between the experimental and theoretical recovery ratios is shown for a range of $\overline{W}$ in Fig. 11. The agreement is encouraging.

Some calculated tangential velocity profiles are shown in Fig. 13.

Primary Flow Beyond the Boundary Layer

Most of the theoretical stability results presented in this memorandum were obtained by assuming that the disturbances are confined to some boundary layer near the outer wall. For such stability calculations, only the primary flow in the boundary layer as obtained above is required. A few stability calculations, however, were made without assuming that the disturbances are confined to any particular part of the flow. We shall call these "finite gap" stability calculations. Then we require also some approximation to the primary flow in the interior of the vortex tube.

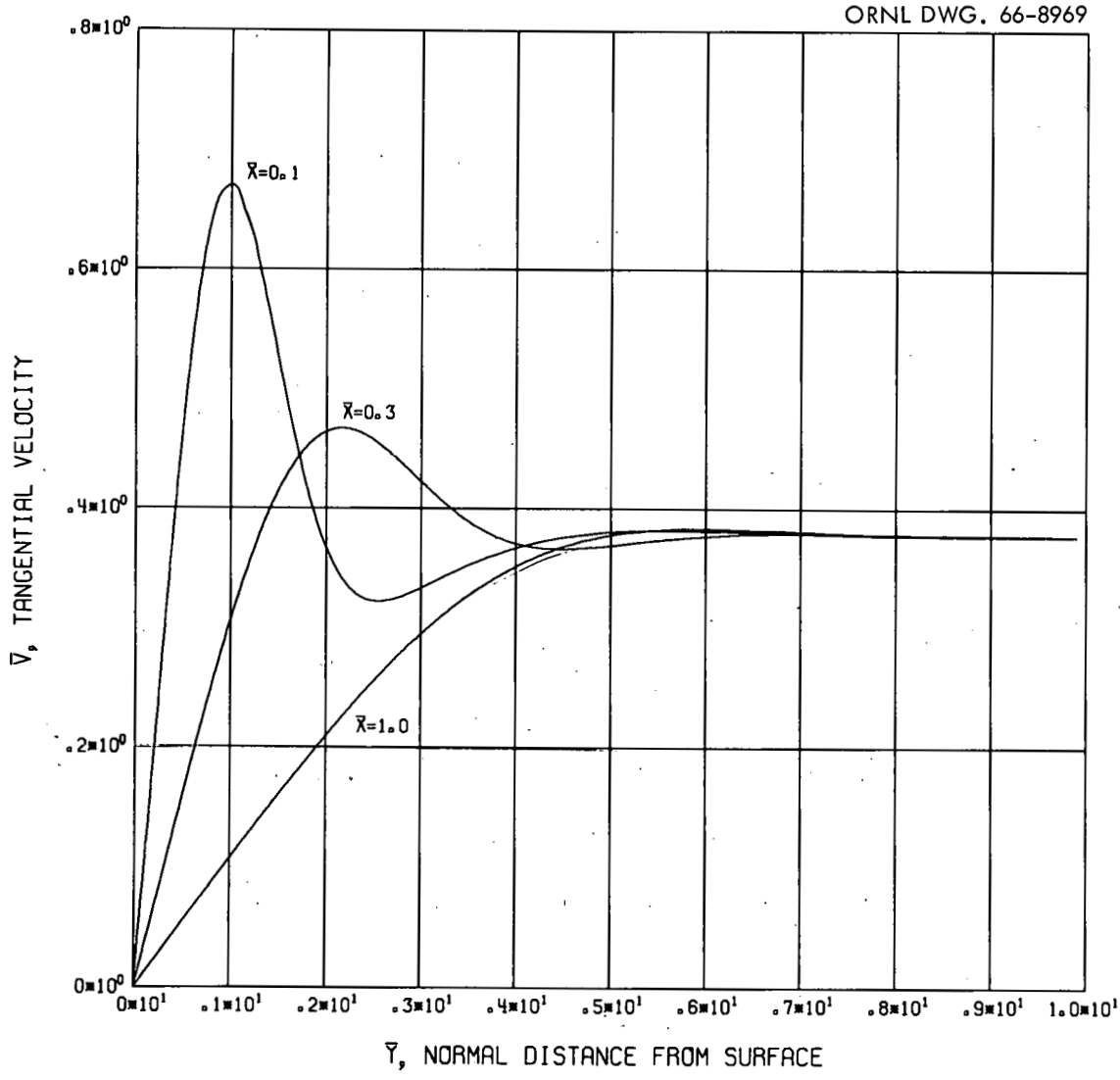

Fig. 13. Jet Boundary-Layer Profiles, $\overline{W}$ = 0.6.

Boundary-layer techniques involve, in effect, an asymptotic expansion of the form

$$U = U_o + U_1\delta + U_2\delta^2 + \cdots \ ,$$

$$V = V_o + V_1\delta + V_2\delta^2 + \cdots \ , \qquad (14)$$

where $U_o = 0$, and give as results the lowest-order non-zero terms V_o and U_1. If we substitute Eq. (14) into Eqs. (12) keeping r and θ as variables for the interior flow, let $\nu = \delta^2 V_j/\ell$, and collect coefficients of the various powers of δ, it is not difficult to show that $V_o \propto 1/r$. Thus, the boundary-layer tangential profile must be faired into a $1/r$ profile in the interior region of the vortex tube. This is done readily by putting

$$V_o(r,\theta) = V_j \frac{r_o}{r} \overline{V}\left(\frac{n\theta}{2\pi}\ , \frac{r_o - r}{\delta}\right) \ . \qquad (15)$$

The radial dependence of U_1 is much more complicated. A partial differential equation describing its behavior in r, θ can be derived, but we shall merely make the crude approximation that

$$U_1(r,\theta) = -V_j \frac{r_o}{r}\frac{1}{\ell}\overline{U}\left(\frac{n\theta}{2\pi}\ , \frac{r_o - r}{\delta}\right) \ , \qquad (16)$$

by analogy with V_o. Equation (16) is accurate within the boundary layer but a poor approximation in the interior region.

For our finite gap stability calculations, we assume

$$U = \delta\ U_1 \qquad \text{and} \qquad V = V_o \ . \qquad (17)$$

Stability

Normal Mode Equations

The first-order perturbation equations [Eqs. (5)] form a set of coupled, linear differential equations governing the perturbations for a given stationary provile (U,V). The perturbations are now resolved into normal modes of the form:

$$\phi(r) \exp(iat) \begin{cases} \sin bz \\ \cos bz \end{cases} , \tag{18}$$

where $\phi(r)$ is the complex amplitude, a is the frequency parameter which may be real, imaginary, or complex, and b is the convective wave number. In terms of the normal modes, Eqs. (5) reduce to a set of coupled, ordinary differential equations governing the complex amplitudes as follows:

$$\left(i\alpha - \frac{L}{N_{Re_j}} + u\frac{d}{dx} + \frac{\partial u}{\partial x}\right) u_1 + \left(\frac{\partial u}{x\partial\theta} - \frac{2v}{x}\right) v_1$$

$$- \frac{\beta}{N_{A\ell}^2} f + \frac{1}{2}\frac{d\pi}{dx} = 0 \quad ,$$

$$\left(\frac{\partial v}{\partial x} + \frac{v}{x}\right) u_1 + \left(i\alpha - \frac{L}{N_{Re_j}} + u\frac{d}{dx} + \frac{u}{x} + \frac{\partial v}{x\partial\theta}\right) v_1 - \frac{\beta}{N_{A\ell}^2} g = 0 \quad , \tag{19}$$

Continued

$$\left(i\alpha - \frac{L + \frac{1}{x^2}}{N_{Re_j}} + u \frac{d}{dx} \right) w_1 + \frac{\beta}{N_{A\ell}^2} h - \frac{\beta}{2} \pi = 0 \quad ,$$

$$\beta u_1 + \left(i\alpha - \frac{L}{N_{Re_m}} + u \frac{d}{dx} - \frac{\partial u}{\partial x} \right) f - \left(\frac{\partial u}{x \partial \theta} \right) g = 0 \quad ,$$

$$\beta v_1 - \left(\frac{\partial v}{\partial x} - \frac{v}{x} \right) f + \left(i\alpha - \frac{L}{N_{Re_m}} + u \frac{d}{dx} - \frac{u}{x} - \frac{\partial v}{x \partial \theta} \right) g = 0 \quad ,$$

$$\frac{du_1}{dx} + \frac{u_1}{x} + \beta w_1 = 0 \quad ,$$

$$\frac{df}{dx} + \frac{f}{x} - \beta h = 0 \quad , \qquad (19)$$

where

$$\alpha = \frac{a r_o}{V_j} \quad , \qquad x = \frac{r}{r_o} \quad , \qquad \beta = b r_o \quad ,$$

$$(U, V)/V_j = (u, v) \quad , \qquad (u', v', w')/V_j = (u_1, v_1, w_1) \quad ,$$

$$(b_r, b_\theta, b_z)/B_o = (f, g, h) \quad , \qquad 2p^*/V_j^2 = \pi \quad ,$$

$$N_{Re_j} = \rho \frac{V_j \, r_o}{\mu} \quad , \qquad N_{A\ell} = \sqrt{\rho \, \mu_o} \; \frac{V_j}{B_o} \quad \text{(Alfvén modulus)} \quad ,$$

$$N_{Re_m} = V_j \, r_o \, \mu_o \, \sigma \quad \text{(magnetic Reynolds modulus)} \quad ,$$

where V_j is the average jet injection velocity, r_o is the radius of curvature of the concave wall, and the operator L is defined as follows:

$$L = \frac{d^2}{dx^2} + \frac{1}{x}\frac{d}{dx} - \frac{1}{x^2} - \beta^2 \quad . \tag{20}$$

These equations must be considered in conjunction with a set of pertinent homogeneous boundary conditions. There appears a major difficulty in the above formulation, however. Since the stationary profile is a function of (x, θ), the coefficients in Eqs. (8) are in general functions of (x, θ). This difficulty is resolved here by considering the stability problem locally, by treating θ as a parameter in the formulation, and carrying out the stability analysis for different constant θ-values. The work of earlier investigators indicates that Görtler instability (unlike Tollmein-Schlichting waves) is determined primarily by the thickness of the boundary layer rather than by detailed shape of the velocity profile. Jet-driven boundary layers increase in thickness as we move downstream from the jet. In the present work, to obtain the lowest values of the critical Görtler

modulus, we shall consider only the stability of the velocity profile at the angular position farthest downstream from the jet.

Reduction of the Normal Equations

In the present problem, the dimensionless stationary profile is taken to be the one obtained using the boundary-layer approximation previously described. In addition, it is assumed that (1) the critical perturbation is that due to a stationary secondary flow [i.e., $\alpha = 0$], and (2) the magnetic Prandtl modulus [N_{Pr_m}] is small.

Under these assumptions, the normal mode equations [Eqs. (19)] reduce to the following set of two coupled differential equations:

$$L^2 u_1 - N_{Re_j} \left(u \frac{d}{dx} + \frac{du}{dx} \right) Lu_1 + \beta^2 Qu_1 - \beta^2 N_{Ta} vLg_1 = 0 \quad ,$$

$$L^2 g_1 - N_{Re_j} \left[u \left(\frac{d}{dx} + \frac{1}{x} \right) - \left(\frac{du}{dx} + \frac{u}{x} \right) \right] Lg_1 + \beta^2 Qg_1 - \left(\frac{dv}{dx} + \frac{v}{x} \right) u_1 = 0 \quad , \tag{21}$$

where

$$Q = \frac{N_{Re_j} N_{Re_m}}{N_{A\ell}^2} \quad ,$$

$N_{Ta} = 2 N_{Re_j}^2$ (Taylor modulus), and

$$g_1 = \frac{g}{N_{Re_j} N_{Re_m} \beta} \quad .$$

Boundary Conditions

The vortex tube is assumed to be nonpermeable and a perfect electrical conductor. To avoid the problem of dealing with the three-dimensional primary flow near the axis, we assume that fluid is removed through a porous inner cylinder of radius, r_1, which rotates at the local tangential fluid velocity, $V(r_1)$. Assuming that the inner cylinder is also perfectly conducting and has a porosity too small to permit appreciable penetration of the disturbance, we have as boundary conditions:

$$u_1 = \frac{du_1}{dx} = \frac{dg_1}{dx} + \frac{g_1}{x} = Lg_1 = 0 \quad \text{at} \quad x = 1,\kappa \quad , \tag{22}$$

where $\kappa = r_1/r_o$.[11]

Solution of Finite-Gap Equations

The stability equations were rewritten as a system of first-order equations and were solved by forward integration using fourth-order predictor-corrector formulas. The method used to calculate the critical values of β and N_{Ta} is described in Ref. 11. The step-size for numerical integration was progressively halved until the critical values of both β and N_{Ta} in two successive calculations differed by less than 1%. As mentioned earlier, however, the error in the calculation of the primary velocity profile was not so carefully controlled. It is probably much larger and may dominate the final error.

Results in terms of the critical Görtler and Hartmann moduli for the case of $\bar{W} = 3.0$, $\kappa = 0.25$, and $n = 2$ are shown in Fig. 14.

---

†See Section 4 for definitions of the Görtler and Hartmann moduli.

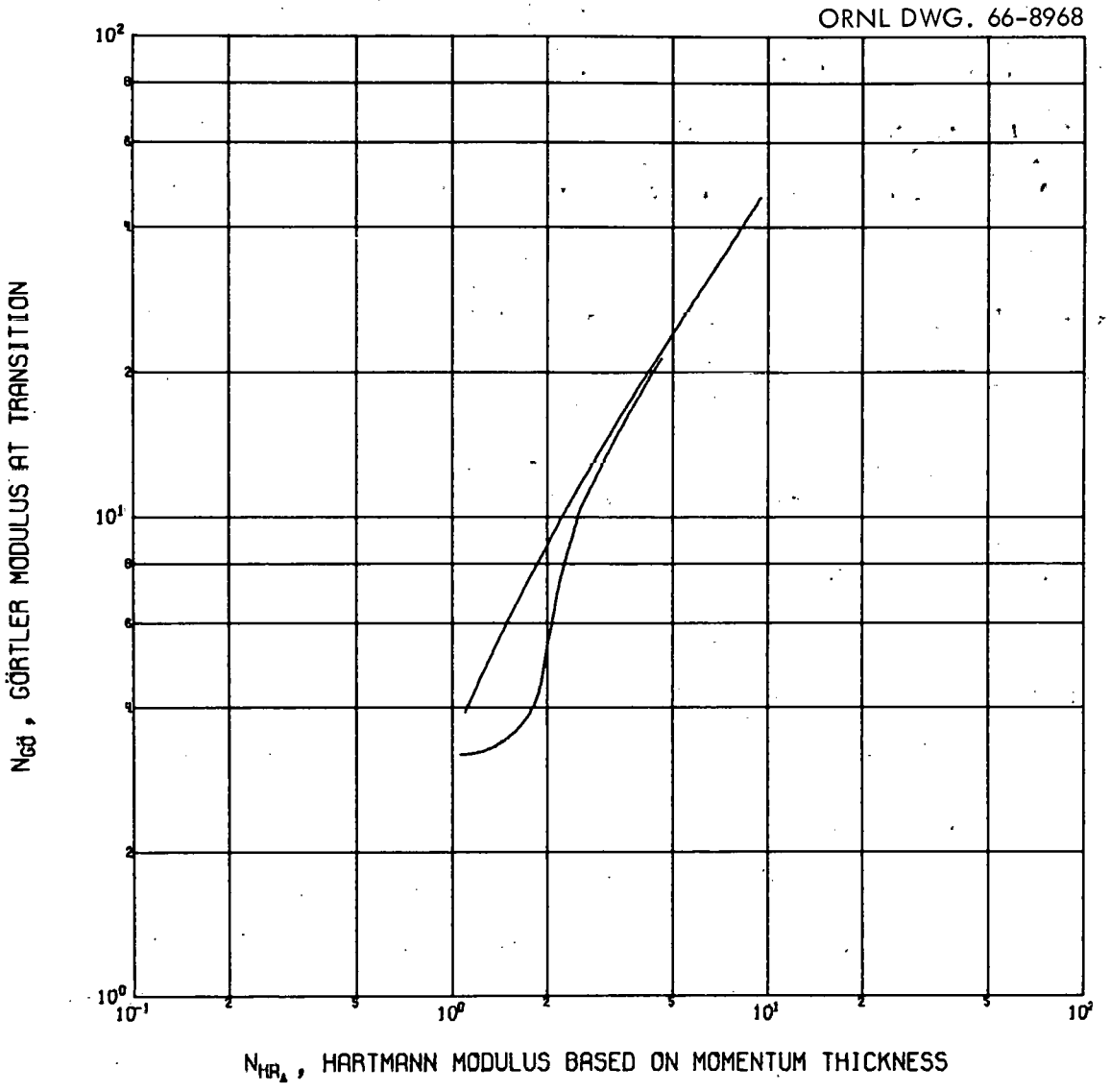

Fig. 14. Comparison of Theoretical Results. Upper curve from boundary-layer stability theory with $\overline{W} = 3.0$. Lower curve from finite-gap theory with two jets. $\kappa = 0.25$, $\overline{W} = 3.0$.

The Görtler modulus, $N_{G\ddot{o}}$, has approximately a constant value of 3 for small values of the Hartmann modulus, N_{Ha_Δ}. Near $N_{Ha_\Delta} = 2$, $N_{G\ddot{o}}$ increases rapidly with N_{Ha_Δ} and the disturbance becomes progressively confined to a layer near the outer wall. For $N_{Ha_\Delta} \gtrsim 3$, the finite-gap results approach the boundary-layer results which were obtained by applying the boundary-layer approximations to the disturbances as described below.

Boundary-Layer Stability Equations

If we apply the boundary-layer transformation

$$\bar{Y} = \frac{r_o - r}{\delta} = \frac{1 - x}{\delta/r_o} \quad , \qquad \delta \ll r_o \quad , \tag{23}$$

to Eq. (21), we obtain a boundary-layer form of the stability equations:

$$\bar{L}^2 u_1 - \left(\bar{U} \frac{d}{d\bar{Y}} + \frac{d\bar{U}}{d\bar{Y}}\right) \bar{L}u_1 + \bar{\beta}^2 \bar{Q}\, u_1 - \bar{\beta}^2 \bar{N}_{Ta}\, \bar{V}\, \bar{L}\, g_1 = 0 \quad ,$$

$$\bar{L}^2 g_1 + \left(\bar{U} \frac{d}{d\bar{Y}} - \frac{d\bar{U}}{d\bar{Y}}\right) \bar{L}g_1 + \bar{\beta}^2 \bar{Q}\, g_1 + \left(\frac{d\bar{V}}{d\bar{Y}}\right) u_1 = 0 \quad , \tag{24}$$

where

$$L = \left(\frac{d^2}{d\bar{Y}^2} - \bar{\beta}^2\right) \quad ,$$

$$\beta = \beta\delta/r_o \quad ,$$

$$\bar{Q} = Q(\delta/r_o)^2 \quad ,$$

$$\bar{N}_{Ta} = N_{Ta}(\delta/r_o)^3 \quad ,$$

$$\bar{u}_1 = u_1 \quad , \text{ and}$$

$$\bar{g}_1 = g_1(r_o/\delta)^3 \quad ,$$

and $\bar{V}$, $\bar{U}$ are the boundary layer primary velocities defined earlier.

As a result of the boundary-layer approximations, the number of the characteristic parameters is decreased by two; and we lose the dependence of the stability criterion on both κ and n.

The boundary conditions become:

$$\bar{u}_1 = \frac{d\bar{u}_1}{d\bar{Y}} = \frac{d\bar{g}_1}{d\bar{Y}} = \bar{L}\bar{g}_1 = 0 \text{ at } \bar{Y} = 0 \quad . \tag{25}$$

In addition, we require that the perturbations $\bar{u}_1$, $\bar{g}_1$, vanish as $\bar{Y} \to \infty$. It is possible to express these boundary conditions such that they can be applied at the outer edge of the boundary layer rather than at infinity, thus restricting the integration to a finite interval. The method is a direct extension of that used by Hämmerlin[21] for his non-magnetic, parallel flow analysis of boundary-layer stability.

The resulting boundary conditions are:

$$\left[\left(\frac{d}{d\bar{Y}}\right)^2 + \left(m_1 + m_2\right)\frac{d}{d\bar{Y}} + m_1 m_2\right]\bar{u}_1 - \left[M\frac{d}{d\bar{Y}} + N\right]\bar{g}_1 = 0 \quad , \tag{26}$$

Continued

$$\left[\left(\frac{d}{d\bar{Y}}\right)^2 - \left(m_1 + m_2\right)\frac{d}{d\bar{Y}} + m_1 m_2\right]\bar{g}_1 = 0 \quad ,$$

$$\left[\left(\frac{d}{d\bar{Y}}\right)^3 - \left(m_1 + m_2\right)\left(\frac{d}{d\bar{Y}}\right)^2 + m_1 m_2 \left(\frac{d}{d\bar{Y}}\right)\right]\bar{u}_1$$

$$-\left[M\left(\frac{d}{d\bar{Y}}\right)^2 + N\left(\frac{d}{d\bar{Y}}\right)\right]\bar{g}_1 = 0 \quad ,$$

$$\left[\left(\frac{d}{d\bar{Y}}\right)^3 - \left(m_1 + m_2\right)\left(\frac{d}{d\bar{Y}}\right)^2 + m_1 m_2 \left(\frac{d}{d\bar{Y}}\right)\right]\bar{g}_1 = 0 \quad , \qquad (26)$$

where

$$M = \frac{2FH + FG(m_1 + m_2) + EH(m_1 + m_2) + 2GE\, m_1 m_2}{F^2 + FE(m_1 + m_2) + E^2\, m_1 m_2} \quad ,$$

$$N = \frac{1}{F}\left[EM\, m_1 m_2 - H(m_1 + m_2) - 2G\, m_1 m_2\right] \quad ,$$

$$E = 4\left[(m_1 + m_2)^2 - m_1 m_2\right] - 4\bar{\beta}^2 + 3\bar{U}_\infty\,(m_1 + m_2) \quad ,$$

$$F = -4\, m_1\, m_2(m_1 + m_2) + \bar{U}_\infty(-3m_1\, m_2 - \bar{\beta}^2) \quad ,$$

$$G = \bar{\beta}^2\, \bar{N}_{Ta}\, \bar{V}_\infty\,(m_1 + m_2) \quad ,$$

$$H = \bar{\beta}^2\, \bar{N}_{Ta}\, \bar{V}_\infty\,(-m_1 m_2 - \bar{\beta}^2) \quad ,$$

m_1, m_2 are the roots with negative real parts of the polynomial equation

$$(m^2 - \bar{\beta}^2)^2 - \bar{U}_\infty\, m(m^2 - \bar{\beta}^2) + \bar{\beta}^2\, \bar{Q} = 0 \quad ,$$

$$\overline{V}_\infty = \lim_{\overline{Y} \to \infty} \overline{V} \quad ,$$

and

$$\overline{U}_\infty = \lim_{\overline{Y} \to \infty} \overline{U} \quad .$$

Equations (26) may be applied at any value of $\overline{Y}$ such that $\overline{V} = \overline{V}_\infty$ and $\overline{U} = \overline{U}_\infty$. In practice, these conditions were usually applied at the value $\overline{Y}_{max}$ used in the primary flow calculations.

Boundary-Layer Stability Results

The boundary-layer stability equations were solved by numerical integration in the same way as the finite-gap equations.

Figure 15 shows the critical or transition value of $N_{G\ddot{o}}$ as a function of N_{Ha_Δ} for $\overline{W} = 0.6$. For large N_{Ha_Δ}, the curve approaches a straight line and $N_{G\ddot{o}} \propto N_{Ha_\Delta}$. For small N_{Ha_Δ}, $N_{G\ddot{o}}$ decreases without appearing to approach a finite lower limit, at least for the range of N_{Ha_Δ} considered.

Figure 16 shows the critical value of the wave number

$$\beta_\Delta = \Delta b \quad , \tag{27}$$

based on the momentum thickness, Δ, as a function of N_{Ha_Δ}. For large N_{Ha_Δ}, $\beta_\Delta \propto N_{Ha_\Delta}^{-1}$. For small N_{Ha_Δ}, β_Δ decrease steadily as $N_{Ha_\Delta} \to 0$.

The boundary-layer stability analysis for $\overline{W} = 0.6$ was used to calculate the curve in Fig. 9 labeled "Laminary Boundary-Layer Theory."

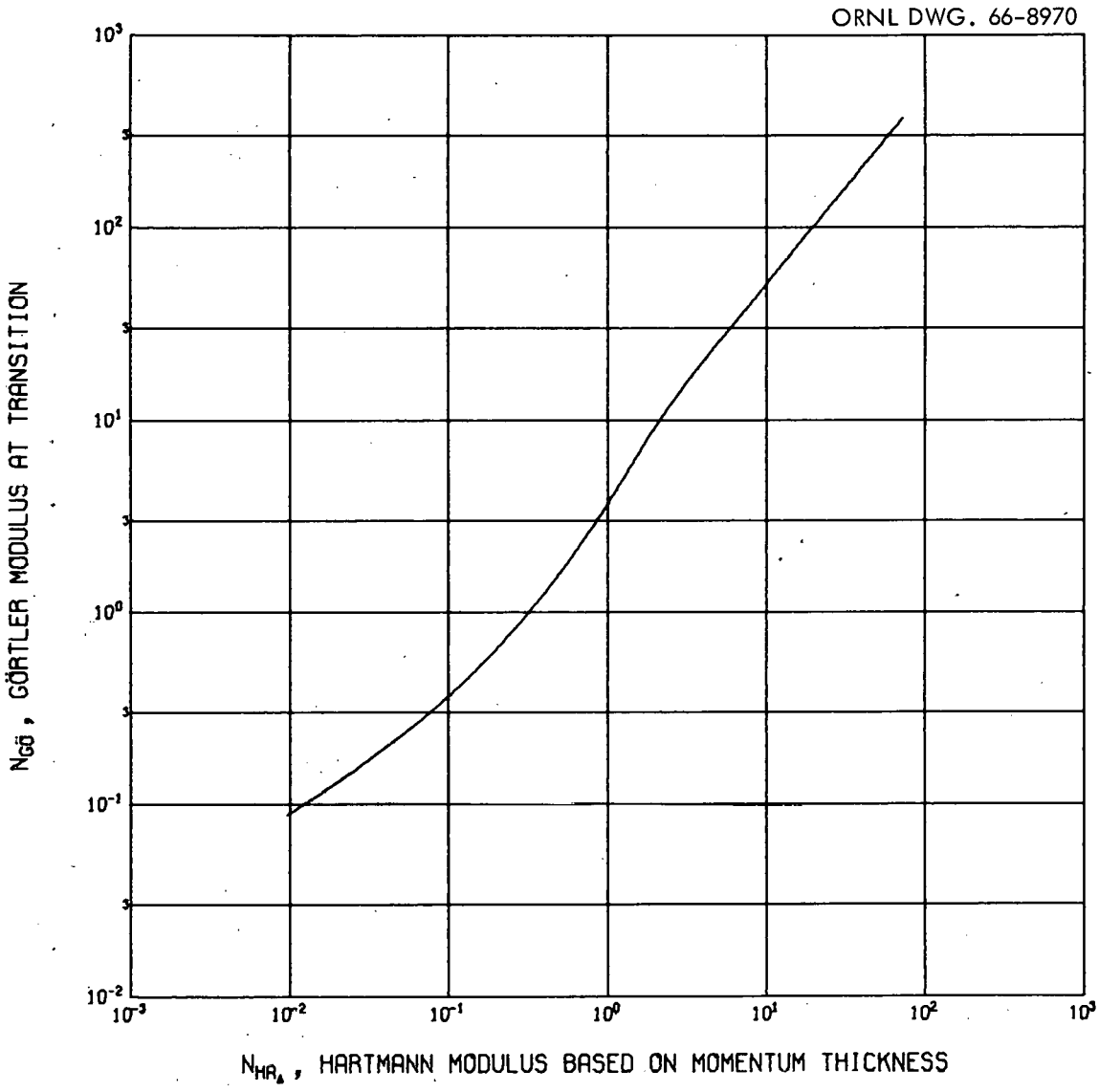

Fig. 15. Critical Görtler Modulus, Theory, $\overline{W} = 0.6$.

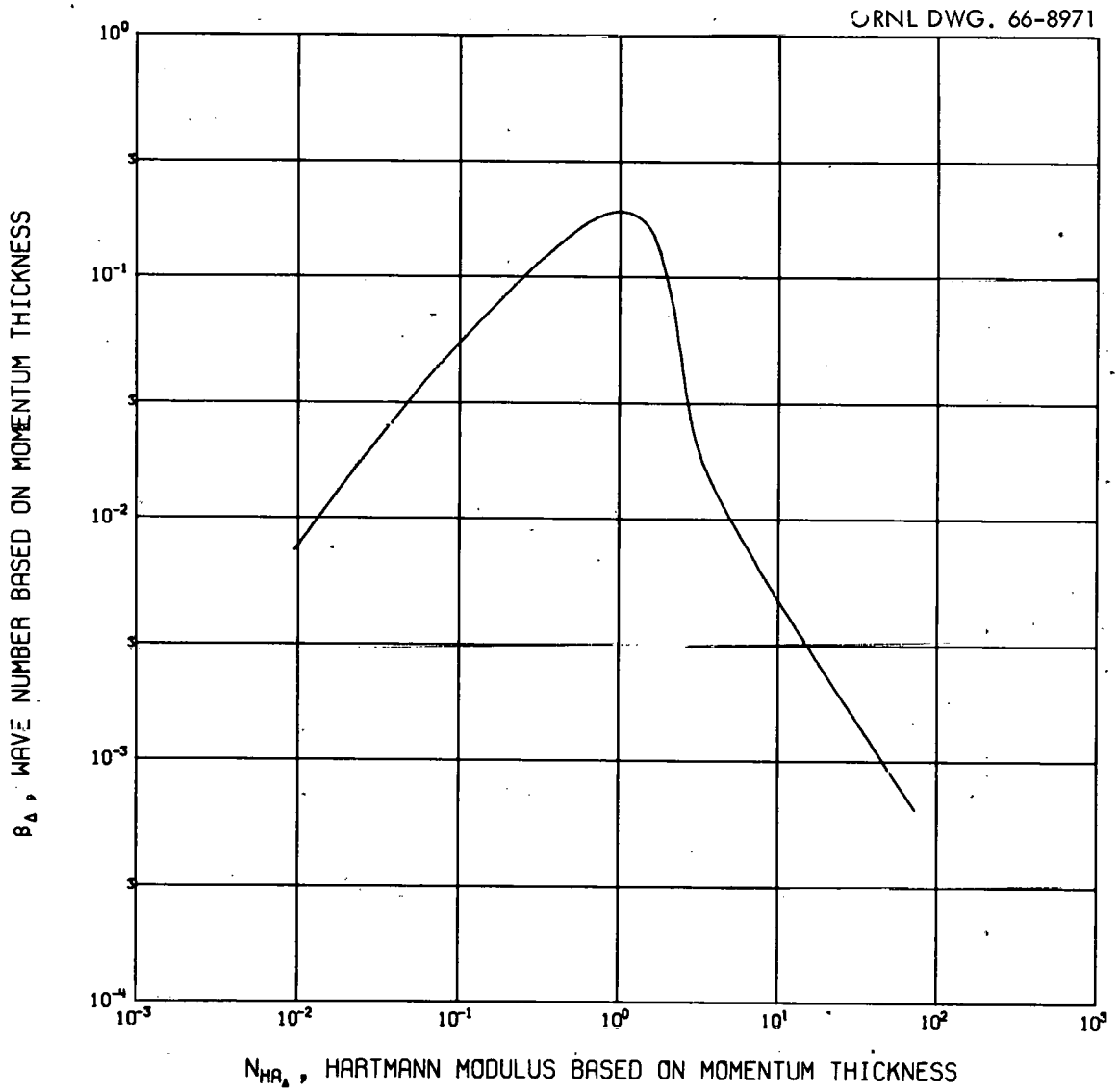

Fig. 16. Critical Wave Number, Theory, $\overline{W} = 0.6$.

Comparison with Previous Theoretical Investigations

The authors know of no previous work on the hydromagnetic Görtler stability problem. The nonmagnetic stability problem has been treated theoretically by Görtler,[16] Hämmerlin,[21] Meksyn,[22] and Smith.[23]

Görtler first proposed and demonstrated theoretically that Taylor instability could occur in a boundary layer on a concave surface. He made the parallel flow approximation (i.e., he neglected the component of the primary velocity normal to the surface) in deriving the stability equations.

Meksyn solved Görtler's stability equations using a different, asymptotic method of integration.

Hämmerlin also resolved Görtler's equations by different methods and apparently obtained very accurate solutions. He first established the peculiar result that the minimum Taylor or Görtler modulus for neutral stability occurs at an axial wave number of zero. The resulting disturbances extend far outside of the boundary layer.

Smith considered the approximations made in deriving the stability equations in detail and derived a new set of much more complicated equations. The additions to the stability equations made by Smith are of three types: (1) Normal flow terms. Certain terms involving the velocity normal to the surface in a growing boundary layer were found to be of the same order of magnitude as the tangential velocity terms. (2) Finite curvature terms. Terms approximately describing the effect of curvature on the disturbances were retained. The addition of these terms involves the introduction of a new parameter, and the relative importance of the terms depends on the range of values chosen for the

new parameter. (3) Growth rate terms. Smith permitted the disturbances to grow in the downstream direction rather than in time. These growth rate terms do not appear in the neutral stability equations.

To clarify the relationship between the present work and that of Smith, we note that we retain the same normal flow terms as Smith. In the finite-gap calculations, we retain finite wall curvature terms without, however, making the approximations used by Smith. In the boundary-layer calculations, we neglect curvature terms. We do not consider finite rates of growth at all.

The results of Görtler, Hämmerlin, and Smith are in general agreement, while the critical results of Meksyn are somewhat higher. Hämmerlin, whose calculations are probably most precise, found a critical Görtler modulus of about 0.31 and a critical wave number of zero for the Blasius profile.

It may be seen from Fig. 15 that at small values of N_{Ha_Δ}, the present calculations using the boundary-layer approximations give critical values of $N_{G\ddot{o}}$ much less than 0.31. To investigate the cause of the very small critical values of $N_{G\ddot{o}}$ obtained, some calculations were made using the present methods for the Blasius profile, neglecting the normal flow terms. The results were in very good agreement with Hämmerlin, with $N_{G\ddot{o}} \to 0.31$ and $\beta_\Delta \to 0$ as $N_{Ha_\Delta} \to 0$. As N_{Ha_Δ} increases, it was found that the growth of the disturbance outside of the boundary was limited by the magnetic field; and a finite critical wave number was obtained.

The calculations were then repeated, still for the Blasius profile, but including the normal flow terms. The critical value of $N_{Go}^{..}$ then became very small as $N_{Ha_\Delta} \to 0$, similar to Fig. 15. The normal flow terms thus seem to have a destabilizing effect on the flow at very small values of N_{Ha_Δ}. As N_{Ha_Δ} increases, however, the importance of the normal flow terms diminishes.

Finally, the neutral stability curve of $N_{Go}^{..}$ versus β_Δ at $N_{Ha_\Delta} = 0$ was calculated for the Blasius profile with the normal flow terms. The results at $\beta_\Delta = 0.664$, where Smith has made particularly detailed calculations, are in good agreement with those of Smith. At very small values of β_Δ, however, $N_{Go}^{..}$ becomes very small.

It seems likely that the effect of the normal flow is to aid in the growth of the disturbance beyond the boundary layer. When an appreciable magnetic field is applied, the perturbed motion outside of the boundary layer is damped in any case; and the normal flow is relatively unimportant.

It is not known defintely why Smith did not find lower values of $N_{Go}^{..}$. It could be because of the finite curvature terms which he retained, or his method of solution (Galerkin's method) which may not have given adequate representation of the disturbances outside of the boundary layer at small wave numbers.

Limits of Applicability of the Theory and Comparison with Experiment

Primary Flow Calculations

To permit the use of the boundary-layer approximations, the Reynolds modulus must be large. If we arbitrarily adopt the criterion

$$V_j \delta/\nu \gtrsim 10 \quad , \tag{28}$$

then in a vortex tube we must have

$$N_{Go}'' \gtrsim 7.5/\sqrt{n} \quad . \tag{29}$$

We also require that the boundary-layer thickness be small compared to the radius of curvature, say:

$$\delta/r_o \lesssim 0.1 \quad , \tag{30}$$

which can be rewritten as

$$N_{Go}'' \gtrsim 19/n \quad . \tag{31}$$

Most of the experimental results are border-line cases with respect to these limits. Nevertheless, agreement between experimental and theoretical recovery ratios is rather good as indicated in Fig. 11.

Finite-Gap Stability Results

All stability calculations require a primary flow and are therefore also limited by the above restrictions. In addition, the finite-gap stability calculations involve a very artificial treatment of the inner boundary condition and require a knowledge of the radial dependence of the primary radial velocity beyond the boundary layer; this has been treated only very crudely in this work.

Comparison of the finite-gap curve of Fig. 14 with the experimental points of Fig. 9 show a rather poor agreement, even in the qualitative shape of the curves.

There are two properties of the finite-gap results which are of interest: (1) At small values of N_{Ha_Δ}, $N_{G\ddot{o}}$ approaches a non-zero limit (which incidentally depends on κ and n) and is well above the boundary-layer stability result. This occurs very simply because the physical dimensions of the vortex tube limit the maximum size of a disturbance which can form, and should therefore be at least qualitatively correct. (2) At large values of N_{Ha_Δ}, the disturbance becomes confined to a thin boundary layer, the difficulties with inner boundary conditions and interior radial flow become unimportant, and the finite-gap results approach the boundary layer results.

Boundary-Layer Stability Results

The validity of the boundary-layer stability results is also limited by Eqs. (29) and (31), however, because of the tendency of the disturbances to extend far beyond the boundary layer, a more stringent limitation than Eq. (31) is probably required when N_{Ha_Δ} is small. In any case, even with the maximum number of four jets used in the experiments, stability results for which $N_{G\ddot{o}}$ is less than three or four should probably be rejected because of the boundary-layer approximations. Poor agreement of the boundary-layer results with experimental data is evident in Fig. 9.

Treatment of the θ-Dependence

Finally, we note that we have ignored the θ-dependence of the disturbance and have considered only the neutral stability at that

value of θ at which the primary velocity profile is believed to be most unstable. This might be interpreted very roughly as meaning that, at the critical Görtler modulus which we calculate, the loss of energy by the disturbance due to dissipation exceeds the energy gain from the primary flow at all values of θ except one, where the energy loss and gain just balance. The true critical Görtler modulus should then be of some higher value, at which the energy loss and gain through the entire flow regime balance. This could account for the low theoretical results shown in Fig. 9. An attempt using an integral growth parameter as suggested by Smith[23] may probably be an improvement over the present theory.

Oscillatory Modes

In earlier theoretical studies of the hydromagnetic stability of Couette flow between conducting cylinders,[12] the authors have reported that, at high values of the Hartmann modulus, disturbances involving an oscillatory time dependence sometimes occur and may become more unstable than the stationary disturbances. For the primary flow considered in the present work, the possibility of the existence of oscillatory critical disturbances has not been adequately investigated. We note, however, that in all earlier cases where oscillatory critical modes occurred, calculations of the most unstable stationary modes led to an abnormal behavior of the critical Taylor modulus and wave number as the Hartmann modulus became very large; the asymptotic behavior of $N_{G\ddot{o}} \propto N_{Ha_\Delta}$ and $\beta_\Delta \propto N_{Ha_\Delta}^{-1}$ as $N_{Ha_\Delta} \to \infty$ of Figs. 15 and 16 is "normal" in this respect.

6. CONCLUSIONS

Experimental

Hydromagnetic studies have been made of vortex flow of an aqueous electrolytic conductor induced by two-dimensional slits oriented tangentially in the wall of a 10-cm-diam by 41-cm-long tube with fluid removal at the center of one end. Flow visualization employing motion-picture photography revealed the transition to an unstable flow which ultimately became turbulent. The principal observations and conclusions of this study are:

1. The transition to instability was observed as a periodic expansion and contraction of a dye trace (as viewed in the axial direction) along the concave wall downstream from a feed slit which occurred when the tangential Reynolds modulus exceeded a certain critical value dependent on the strength of the magnetic field. At values of the tangential Reynolds modulus a few percent above the critical, the dye trace in the vicinity of the wall oscillated with a rather well-defined radial amplitude which increased with the amount by which the critical Reynolds modulus was exceeded. Irregular rolling of the trace around a circumferential streamline was also noted well above the transition point. When the critical Reynolds modulus was exceeded by more than a few percent, the instability developed into a disorganized turbulent-like flow characterized by gross mixing. It should be noted that no significant effect on the nature of the transition as observed in these experiments resulted from application of the magnetic field. While no definite Taylor-type cellular vortices were observed at the transition point in these experiments, it may nevertheless be possible that the Taylor-Görtler mechanism is responsible for the instability; the disturbing

influence of the jets on flow near the wall may have prevented formation of recognizable cells (Fig. 4).

2. The axial magnetic field suppressed the transition to instability. For example, with two injection slits, the critical tangential Reynolds modulus (based on tube radius and tangential velocity at a radius ratio of 0.8) was increased from 500 with no magnetic field to 7600 using a 75-kilogauss axial magnetic field applied to give a Hartmann modulus (based on tube radius) of 172 (Fig. 8).

3. Increasing the number of injection slits (at constant slit width) increased the critical Reynolds modulus but decreased the influence of the field on the critical Reynolds modulus at high values of the Hartmann modulus (Fig. 8).

4. The recovery of injection velocity as tangential velocity near the periphery of the tube was increased significantly when the vortex flow was stabilized by the magnetic field, a result which can be interpreted as being due to a corresponding decrease in wall shear. The stabilized flow data agree very well with results obtained by solving the boundary-layer equations for the steady-state velocity profile as a function of distance from an injection slit, neglecting curvature (Fig. 11).

5. When the tangential Reynolds modulus was raised above the critical value for complete stabilization, the magnetic field was nevertheless effective in stabilizing the interior of the vortex flow. For example, at a tangential Reynolds modulus of 13,200, definite laminar flow was observed inside a radius ratio of about 0.8. Although the flow near the wall remained turbulent in this case, the field was found to inhibit growth of the disturbances, resulting in a decrease in the scale of the turbulence (Figs. 6 and 7).

6. The data for 1-, 2-, and 4-slit injection when compared in terms of the critical "Görtler modulus", $(V^*_{0.8}\ \Delta/\nu)(\Delta/r_o)^{0.5}$, and the Hartmann modulus (based on momentum thickness), $\sqrt{\sigma/\mu}\ B_o\ \Delta$, were found to fall on three distinct curves (Fig. 9). Significant improvement in the correlation resulted by adjusting the exponent on the ratio Δ/r_o in the Görtler modulus from 0.5 to 0.43 (Fig. 10).

Analytical

An MHD Görtler-type stability analysis based on a tangential jet-injection velocity profile over a concave wall has been considered. The stationary jet-injection velocity profile was calculated according to the classical theory of laminar boundary-layer flow, and the stability analysis was carried out numerically based on linear perturbation theory for the calculated profile under the influence of a transverse magnetic field. Most of the theoretical stability results presented in this paper were obtained by a boundary-layer stability analysis; that is, by assuming that the disturbances are confined to some boundary layer of the flow. A few stability calculations, however, were obtained by a finite-gap analysis without assuming that the disturbances are confined to any particular part of the flow. For these calculations, a crude approximation of the flow outside of the boundary layer for a vortex geometry was used.

A typical set of calculated jet-injection, boundary-layer profiles is shown in Fig. 13. Comparison between experimental and theoretical recovery ratio based on the calculated profiles is presented in Fig. 11, in which good agreement is evident.

Comparison of the stability results with experiments is presented in Figs. 9 and 14; here poor agreement is observed. At large values of N_{Ha_Δ},

the boundary-layer and finite-gap stability analyses are nearly equivalent. At small values of N_{Ha_Δ}, the Görtler modulus approaches zero for the boundary-layer analysis and a finite value for the finite-gap analysis. Since the physical dimensions of the vortex tube limit the maximum size of a disturbance, the latter is at least qualitatively correct. However, in order to insure that the jet-injection boundary-layer thickness be small compared to the radius of curvature, the stability theory is applicable only for relatively large values of $N_{G\ddot{o}} \gtrsim 19/n$).

The authors know of no previous work on the hydromagnetic Görtler stability problem. The nonmagnetic stability problem has been treated theoretically by Görtler, Hämmerlin, Meksyn, and Smith. At $N_{Ha_\Delta} \to 0$, the present results indicate that the critical Görtler modulus for a boundary layer falls far below the values obtained by the earlier investigators. The low critical value has been traced to terms in the stability equations which account for normal flow caused by growth of the boundary layer. Without such terms, very good agreement with Hämmerlin could be obtained.

ACKNOWLEDGMENT

The authors wish to express appreciation to Dr. W. F. Gauster and to R. L. Brown, Thermonuclear Division, for their cooperation in making the Magnet Laboratory available for the experiments. R. E. Dial was responsible for design, assembly, and operation of the experiment as well as for data analysis. R. M. Summers measured the viscosity, and Dr. T. R. Mueller the electrical conductivity of the ammonium chloride solutions. Dolores Eden prepared the final manuscript.

REFERENCES

1. W. S. Lewellen and W. R. Grabowsky, Nuclear Space Power Systems Using Magnetohydrodynamic Vortices, ARS Journal, 32: 693 (1962).

2. J. L. Kerrebrock and R. V. Meghreblian, An Analysis of Vortex Tubes for Combined Gas-Phase Fission Heating and Separation of the Fissionable Material, USAEC Report ORNL-CF-57-11-3 (Rev. 1), Oak Ridge National Laboratory, 1958.

3. J. J. Keyes, Jr., and R. E. Dial, An Experimental Study of Vortex Flow for Application to Gas-Phase Fission Heating, USAEC Report ORNL-2837, Oak Ridge National Laboratory, 1960.

4. G. J. Kidd, Jr., Confined Vortex Flow Near a Stationary Disk, USAEC Report ORNL-TM-1387, Oak Ridge National Laboratory, 1966.

5. H. W. Hoffman and J. J. Keyes, Jr., Studies in Heat Transfer and Fluid Mechanics Progress Report for Period January 1 – September 30, 1963, USAEC Report ORNL-TM-915, Oak Ridge National Laboratory, October 1964.

6. J. J. Keyes, Jr., An Experimental Hydrodynamic Investigation of Jet-Driven, Confined Vortex-Type Fluids, pp. 277–296 in Developments in Theoretical and Applied Mechanics, Vol. 2, edited by W. A. Shaw, Pergamon Press, Oxford, 1965 (Proceedings of the Second Southeastern Conference on Theoretical and Applied Mechanics, Atlanta, Georgia, March 5-6, 1964).

7. H. W. Hoffman and J. J. Keyes, Jr., Studies in Heat Transfer and Fluid Mechanics Progress Report for Period October 1, 1963 – June 30, 1964, USAEC Report ORNL-TM-1148, Oak Ridge National Laboratory, August 1965.

8. R. J. Donnelly and M. Ozima, Experiments on the Stability of Flow Between Rotating Cylinders in the Presence of a Magnetic Flow, Proc. Roy. Soc. (London), A266: 272–286 (1962).

9. R. J. Donnelly and D. R. Caldwell, Experiments on the Stability of Hydromagnetic Couette Flow, J. Fluid Mech., 19: 257–263 (1964).

10. S. Chandrasekhar, Hydrodynamic and Magnetohydrodynamic Stability, pp. 411–412, Oxford University Press, New York, 1961.

11. T. S. Chang and W. K. Sartory, Hydromagnetic Stability of Vortex-Like Flow, USAEC Report ORNL-3707, Oak Ridge National Laboratory, 1966.

12. T. S. Chang and W. K. Sartory, Transition from Stationary to Oscillatory Modes of Instability in Magnetohydrodynamic Couette Flow, USAEC Report ORNL-TM-1404, Oak Ridge National Laboratory, 1966.

13. L. R. Boedeker and E. E. Covert, Measurements of Helical Flow of a Strong Electrolyte With and Without a Magnetic Field, Report AFOSR-2806, MIT Aerophysics Laboratory, 1962.

14. R. A. Armistead, Jr., Turbulence-Induced Heat-Transfer Fluctuations in Pipe Flow of Water Using Hot-Film Wall Sensors, USAEC Report ORNL-TM-1602, Oak Ridge National Laboratory, 1966 (Ph.D. Dissertation, Carnegie Institute of Technology, Pittsburgh, Pennsylvania).

15. G. I. Taylor, Stability of a Viscous Liquid Contained Between Two Rotating Cylinders, Phil. Trans. Roy. Soc. (London), A223: 289–343 (1923).

16. H. Gortler, Über eine dreidimensionale Instabilität laminarer Grenzschichten an konkaven Wänden, Nachr. Wiss. Ges. Göttingen, Math. Phys. Klasse, New Series 2, No. 1 (1940).

17. F. R. Hama, J. D. Long, and J. C. Hegarty, On Transition from Laminar to Turbulent Flow, J. Appl. Phys., 28: 388–394 (1957).

18. H. Schlichting, Boundary Layer Theory, 4th ed., Chap. VII, p. 123, McGraw-Hill Book Company, Inc., New York, 1960.

19. M. P. Lietzke, Polfit II – An IBM 7090 Program for Polynominal Least-Squares Fitting, USAEC Report ORNL-3132, Oak Ridge National Laboratory, 1961.

20. H. Schlichting, Boundary Layer Theory, 4th ed., Chap. XVII, pp. 440–444, McGraw-Hill Book Company, Inc., New York, 1960.

21. G. Hämmerlin, Über das Eingenwertproblem der dreidimensionalen Instabilität laminarer Grenzschichten an konkaven Wänden, Diss. Freiburg 1954., J. Rat. Mech. and Anal., 4: 279–321 (1955).

22. D. Meksyn, Stability of Viscous Flow Over Concave Cylindrical Surfaces, Proc. Roy. Soc. (London), A203: 253–265 (1950).

23. A. M. O. Smith, On the Growth of Taylor Görtler Vortices Along Highly Concave Walls, Quart. Appl. Math., 13: 223–262 (1955).

INTERNAL DISTRIBUTION

1. L. G. Alexander
2. S. E. Beall
3. C. A. Brandon
4-8. T. S. Chang
9. J. W. Cooke
10. W. B. Cottrell
11. F. L. Culler
12. J. A. Edwards
13. A. P. Fraas
14. W. R. Gambill
15. P. N. Haubenreich
16-20. H. W. Hoffman
21. P. R. Kasten
22-26. J. J. Keyes, Jr.
27. G. J. Kidd, Jr.
28. J. K. Jones
29. C. G. Lawson
30. M. I. Lundin
31. R. N. Lyon
32. R. E. MacPherson
33. H. G. MacPherson
34. H. C. McCurdy
35. A. J. Miller
36. A. M. Perry
37. T. T. Robin, Jr.
38. M. W. Rosenthal
39-43. W. K. Sartory
44. A. W. Savolainen
45. M. J. Skinner
46. I. Spiewak
47. D. G. Thomas
48. D. B. Trauger
49. J. S. Watson
50. A. M. Weinberg
51. G. D. Whitman
52. R. P. Wichner
53. G. Young
54-55. Central Research Library (CRL)
56-57. Y-12 Document Reference Section (DRS)
58-60. Laboratory Records Department (LRD)
61. Laboratory Records Department – Record Copy (LRD-RC)

EXTERNAL DISTRIBUTION

62. D. R. Bartz, Jet Propulsion Laboratory, Pasadena, California
63. J. R. Beyster, General Atomic, San Diego, California
64. C. J. Bridgman, Air Force Institute of Technology, Wright-Patterson Air Force Base, Ohio
65. J. A. Brousseau, The Boeing Company, Seattle, Washington
66. W. G. Burwell, United Aircraft Corporation, Research Laboratories, East Hartford, Connecticut
67. R. W. Bussard, Electro-Optical Systems, Inc., Pasadena, California
68. James Carton, REON Division, Aerojet-General Corporation, Sacramento, California
69. C. C. Chang, Catholic University of America, Washington, D. C.
70. Peter Chiarulli, Illinois Institute of Technology, Chicago, Illinois
71. Joseph Clement, Georgia Institute of Technology, Atlanta, Georgia
72. Ralph S. Cooper, Donald W. Douglas Laboratories, Richland, Washington
73. J. S. Cory, Donald W. Douglas Laboratories, Richland, Washington
74. H. F. Crouch, Lockheed Missiles & Space Company, Space Systems Division, Sunnyvale, California
75. J. P. Davis, Jet Propulsion Laboratory, Pasadena, California
76. Robert Dillaway, Rocketdyne, Canoga Park, California
77. D. W. Drawbaugh, Astronuclear Laboratory, Westinghouse Electric Corporation, Pittsburgh, Pennsylvania
78. F. C. Durant, III, National Air Museum, Smithsonian Institute, Washington, D. C.
79. Andrew Fejer, Illinois Institute of Technology, Chicago, Illinois

80. W. M. Foley, United Aircraft Corporation, Research Laboratories, East Hartford, Connecticut
81. R. H. Fox, Institute for Defense Analysis, Arlington, Virginia
82. L. A. Gore, Space Technology Laboratories, Redondo Beach, California
83. Jerry Grey, Grey-Rad Corporation, Princeton, New Jersey
84. R. A. Gross, School of Engineering & Applied Science, Columbia University, New York, New York
85. A. V. Grosse, Research Institute of Temple University, Philadelphia, Pennsylvania
86. George Grover, Los Alamos Scientific Laboratory, Los Alamos, New Mexico
87. S. V. Gunn, Rocketdyne Division of North American Aviation, Canoga Park, California
88. Elias P. Gyftopoulos, Massachusetts Institute of Technology, Cambridge, Massachusetts
89. J. W. Hadley, Lawrence Radiation Laboratory, Livermore, California
90. L. P. Hatch, Brookhaven National Laboratory, Upton, Long Island, New York
91. C. J. Heindly, Jet Propulsion Laboratory, Pasadena, California
92. R. J. Holl, Missiles & Space Systems Division, Douglas Aircraft Company, Santa Monica, California
93. W. J. Houghton, Aerojet-General Corporation, Sacramento, California
94. Henry Hunter, Space Technology Laboratories, Redondo Beach, California
95. Maxwell Hunter, Lockheed Missiles & Space Company, Sunnyvale, California
96. Abraham Hyatt, 1700 E. Imperial Highway, El Segundo, California
97. Kurt P. Johnson, Advanced Space Technology, A2-263, Douglas Missiles & Space Systems Division, Santa Monica, California
98. Carmen Jones, Rocketdyne Division of North American Aviation, Canoga Park, California
99. W. Y. Jordan, Jr., Planetary & Nuclear Systems Group, Advanced Systems Office R-AS, Marshall Space Flight Center, Huntsville, Alabama
100. Larry Kaufman, Manlabs, Inc., Cambridge, Massachusetts
101. Lt. Col. M. R. Keller, Aerospace Research Laboratories (ARN), Wright-Patterson Air Force Base, Ohio
102. J. L. Kerrebrock, Massachusetts Institute of Technology, Cambridge, Massachusetts
103. D. E. Knapp, Donald W. Douglas Laboratories, Richland, Washington
104. Walter F. Krieve, TRW Systems, Redondo Beach, California
105. George T. Lalos, U. S. Naval Ordnance Laboratory, White Oaks, Silver Springs, Maryland
106. Zalman Lavan, Illinois Institute of Technology, M.A.E. Department, Technology Center, Chicago, Illinois
107. David Mallon, Allison Division, General Motors Corporation, Indianapolis, Indiana
108. Edward Mason, Massachusetts Institute of Technology, Cambridge, Massachusetts

109. G. H. McLafferty, United Aircraft Corporation, Research Laboratories, East Hartford, Connecticut
110. R. V. Meghreblian, Jet Propulsion Laboratory, Pasadena, California
111. James Nance, General Atomic, San Diego, California
112. Clyde Orr, Jr., Chemical Engineering Department, Georgia Institute of Technology, Atlanta, Georgia
113. Frank S. Owen, United Aircraft Corporation, Research Labortories, East Hartford, Connecticut
114. Donald Parks, General Atomics Division, General Dynamics Corp., San Diego, California
115. R. W. Patch, Nuclear Systems Division, NASA Lewis Research Center, Cleveland, Ohio
116. John C. Peak, General Atomics Division, General Dynamics Corp., San Diego, California
117. Rafael Perez, Nuclear Engineering Department, University of Florida, Gainesville, Florida
118. H. C. Perkins, Aerospace & Mechanical Engineering Department, University of Arizona, Tucson, Arizona
119. Ben Pinkel, RAND Corporation, Santa Monica, California
120. Robert G. Ragsdale, Nuclear Systems Division, NASA Lewis Research Center, Cleveland, Ohio
121. Frank E. Rom, Nuclear Systems Division, NASA Lewis Research Center, Cleveland, Ohio
122. Jacob B. Romero, Chemical Engineering Department, University of Idaho, Moscow, Idaho
123. Richard Rosa, AVCO Everett Research Laboratory, Everett, Massachusetts
124. Martin Rosenzweig, Aerodynamic & Heat Transfer Department, Aerospace Corporation, Los Angeles, California
125. Eli B. Roth, A. C. Electronics Division, Milwaukee, Wisconsin
126. S. M. Scala, General Electric Company, Space Sciences Laboratory, Philadephia, Pennsylvania
127. F. C. Schwenk, AEC-NASA Space Nuclear Propulsion Office, USAEC, Washington, D. C.
128-129. R. M. Scroggins, AEC, Washington, D. C.
130. W. L. Snapp, Aerojet-General Corporation, Cleveland, Ohio
131. C. K. Soppet, Nuclear Integration Department, REON Division, Aerojet-General Corporation, Sacramento, California
132. R. J. Spindler, AVCO Corporation, Missile Systems Division, Wilmington, Massachusetts
133. J. C. Stewart, University of Colorado, Joint Institute for Laboratory Astrophysics, Boulder, Colorado
134. J. J. Stewart, Aerojet-General Corporation, Sacramento, California
135. Henry Stumpf, Space Sciences Division, Jet Propulsion Laboratory, Pasadena, California
136. T. Szekely, Space Technology Laboratories, Redondo Beach, California
137. Theodore B. Taylor, Defense Atomic Support Agency, Pentagon, Washington, D. C.
138. T. P. Torda, Illinois Institute of Technology, M.A.E. Department, Technology Center, Chicago, Illinois

139. Robert F. Trapp, Biotechnology & Human Research Division, NASA, Washington, D. C.
140. Robert Uhrig, Department of Nuclear Engineering, University of Florida, Gainesville, Florida
141. Hans von Ohain, Aerospace Reaseach Laboratories (ARD-1), Wright-Patterson Air Force Base, Ohio
142. Herbert Weinstein, Chemical Engineering Department, Illinois Institute of Technology, Chicago, Illinois
143. E. P. Wigner, Department of Physics, Princeton University, Princeton, New Jersey
144. Captain William Yingling, AEC-NASA Space Nuclear Propulsion Office, USAEC, Washington, D. C.
145. Jerrold M. Yos, AVCO Corporation, Research & Advance Development Division, Wilmington, Massachusetts
146. M. J. Zucrow, Atkins Professor of Engineering, Mechanical Engineering Department, Purdue University, Lafayette, Indiana
147-161. Division of Technical Information Extension (DTIE)
162. Research and Development Division, ORO
163-164. Reactor Division, ORO